

ARTICLE

Received 12 Dec 2015 | Accepted 20 Jul 2016 | Published 31 Aug 2016

DOI: 10.1038/ncomms12658

OPEN

# Neutrophil recruitment limited by high-affinity bent $\beta_2$ integrin binding ligand in *cis*

Zhichao Fan<sup>1</sup>, Sara McArdle<sup>1,2</sup>, Alex Marki<sup>1</sup>, Zbigniew Mikulski<sup>1</sup>, Edgar Gutierrez<sup>3</sup>, Britta Engelhardt<sup>4</sup>, Urban Deutsch<sup>4</sup>, Mark Ginsberg<sup>5</sup>, Alex Groisman<sup>3</sup> & Klaus Ley<sup>1,2</sup>

Neutrophils are essential for innate immunity and inflammation and many neutrophil functions are  $\beta_2$  integrin-dependent. Integrins can extend ( $E^+$ ) and acquire a high-affinity conformation with an 'open' headpiece ( $H^+$ ). The canonical switchblade model of integrin activation proposes that the  $E^+$  conformation precedes  $H^+$ , and the two are believed to be structurally linked. Here we show, using high-resolution quantitative dynamic footprinting (qDF) microscopy combined with a homogenous conformation-reporter binding assay in a microfluidic device, that a substantial fraction of  $\beta_2$  integrins on human neutrophils acquire an unexpected  $E^-H^+$  conformation.  $E^-H^+$   $\beta_2$  integrins bind intercellular adhesion molecules (ICAMs) in *cis*, which inhibits leukocyte adhesion *in vitro* and *in vivo*. This endogenous anti-inflammatory mechanism inhibits neutrophil aggregation, accumulation and inflammation.

<sup>1</sup>Division of Inflammation Biology, La Jolla Institute for Allergy and Immunology, 9420 Athena Circle Drive, La Jolla, California 92037, USA. <sup>2</sup>Department of Bioengineering, University of California San Diego, 9500 Gilman Drive, La Jolla, California 92093, USA. <sup>3</sup>Department of Physics, University of California San Diego, 9500 Gilman Drive, La Jolla, California 92093, USA. <sup>4</sup>Theodor Kocher Institute, University of Bern, 1 Freiestrasse, 3012 Bern, Switzerland. <sup>5</sup>Department of Medicine, University of California San Diego, 9500 Gilman Drive, La Jolla, California 92093, USA. Correspondence and requests for materials should be addressed to K.L. (email: klaus@lji.org).

Neutrophils are the most abundant leukocyte population in humans and have essential roles in innate immunity and inflammation. Neutrophils form a primary line of defence against pathogens by recognizing, trapping and eliminating bacteria<sup>1</sup>, fungae<sup>2</sup>, viruses<sup>3</sup> and helminths<sup>4</sup> through mechanisms including phagocytosis<sup>5</sup>, superoxide production<sup>5</sup>, granule exocytosis<sup>6</sup> and neutrophil extracellular traps<sup>1</sup>. Congenital deficiencies of neutrophil function, such as leukocyte adhesion deficiency syndrome, can result in fatal infection<sup>7</sup>. Delay in neutrophil recovery is the main reason for lethal infections in patients receiving allogeneic haematopoietic stem cell transplantation<sup>8</sup>. Neutrophils are also important in non-infectious or chronic inflammation such as injury-induced sterile inflammation<sup>9</sup>, and in autoimmune diseases, including rheumatoid arthritis<sup>10</sup>, multiple sclerosis<sup>11</sup> and systemic lupus erythematosus<sup>12</sup>.

Neutrophils are distributed by the blood circulation, but exert most of their functions outside the vascular system, exiting the circulation at sites of inflammation through the classical adhesion cascade<sup>13,14</sup>. Neutrophils have evolved specialized systems to allow adhesion under high wall shear stress<sup>13,15,16</sup>.  $\beta_2$  integrins are vital for neutrophil functions, including neutrophil arrest under flow<sup>13</sup>, transmigration through the vascular endothelium<sup>17</sup>, chemotaxis<sup>18</sup> and phagocytosis<sup>19</sup>.

The leukocyte adhesion cascade was first established when Lawrence and Springer showed that neutrophils rolling on P-selectin were induced to arrest under flow by binding to intercellular adhesion molecule-1 (ICAM-1), a ligand for  $\beta_2$  integrins when the chemoattractant *N*-formylmethionine-leucyl-phenylalanine was infused<sup>14</sup>. Similar results were shown for neutrophil rolling and arrest *in vivo*<sup>20</sup> and in flow chamber studies in which the chemokine interleukin (IL)-8 was co-immobilized with ICAM-1 and P-selectin<sup>21</sup>. Rolling neutrophils arrest by  $\beta_2$  integrin<sup>22</sup> activation through inside-out signalling<sup>23</sup>, which is thought to be rapid and local<sup>24</sup>; however, the subcellular distribution of integrin activation is unknown.

Integrins are  $\alpha\beta$  heterodimers that regulate their adhesiveness through changes in the conformation of their ectodomain<sup>25,26</sup>. Resting integrins assume a bent conformation with low affinity for ligand. The 'switchblade' model of integrin activation (Supplementary Fig. 1a)<sup>25</sup> suggests a two-step activation process in which integrin extension ( $E^+$ ) is followed by a rearrangement in the ligand-binding site leading to high-affinity ( $H^+$ ).  $\beta_2$  integrin extension is detected by monoclonal antibody (mAb) KIM127, which recognizes a neoepitope<sup>27</sup> that is hidden in the bent knee of human  $\beta_2$  (ref. 28). On the other hand, when human  $\beta_2$  integrins acquire high affinity, a neoepitope in the  $\beta_2$  I-like domain<sup>29-31</sup> is exposed, which is recognized by mAb24 (ref. 32). Thus, KIM127 binding indicates  $E^+$  and mAb24 binding indicates  $H^+$ . KIM127 and mAb24 do not block each other and do not block ligand binding.

Research has shown that P-selectin glycoprotein ligand-1 (PSGL-1) signalling triggers integrin extension<sup>33,34</sup>. This signalling cascade starts with L-selectin and PSGL-1 (ref. 35), proceeds through various signalling intermediates<sup>26,34</sup> and induces the  $E^+$  but not the  $H^+$  integrin conformation<sup>33,34</sup>. Another signalling cascade is triggered when a chemokine binds to its cognate G-protein-coupled receptor<sup>26</sup>. This binding induces dissociation of  $G\alpha_{12}$  from  $G\beta\gamma$ , and is required for arrest<sup>36</sup>. A distal signalling cassette involving Rap-1, Rho<sup>37</sup>, Rap1-GTP-interacting adaptor molecule<sup>38,39</sup>, talin<sup>40,41</sup> and kindlin-3 (refs 7,41) has been described. G-protein-coupled receptor signalling is thought to trigger  $H^+$  or possibly both  $E^+$  and  $H^+$  (ref. 23).

Quantitative dynamic footprinting (qDF) microscopy, which is based on variable angle total internal reflection fluorescence

(TIRF) to provide nanometer resolution in the vertical *z* axis, was combined with microfluidics<sup>15,16</sup> to study neutrophil interaction with defined molecular substrates at the subcellular level. This method provides precise maps of the neutrophil surface and the location of relevant molecules. Here we modify and expand qDF microscopy to three colours and combine it with a homogeneous binding assay<sup>33</sup>, which introduces soluble, fluorescence-labelled mAb24 and KIM127, to investigate the dynamics of  $\beta_2$  integrin activation during primary human neutrophil rolling and arrest under physiologic conditions. We find an unexpected  $E^-H^+$  conformation of  $\beta_2$  integrins that interacts with ICAMs *in cis*. This *cis* interaction inhibits leukocyte adhesion and aggregation, thus providing an auto-inhibitory mechanism that curbs inflammatory responses.

## Results

**$\beta_2$  integrin activation on rolling human neutrophils.** Microfluidic chambers<sup>15</sup> were coated with recombinant human P-selectin-Fc (to support rolling), ICAM-1-Fc (a ligand for both  $\alpha_L\beta_2$ , lymphocyte function-associated antigen (LFA)-1 and  $\alpha_M\beta_2$ , macrophage-1 antigen, Mac-1) and IL-8 with all concentrations titrated so that neutrophils would arrest only when all three molecules were present (Supplementary Fig. 2a). Both LFA-1 and Mac-1 contributed to human neutrophil arrest (Supplementary Fig. 2a). Soluble KIM127 and mAb24 did not show any significant influence on neutrophil rolling and arrest (Supplementary Fig. 2b-e). Both antibodies bound rapidly (within one video frame) to immobilized activated neutrophils (Supplementary Fig. 3) with no evidence for the loss of binding over time, underscoring the validity of the homogeneous binding assay. Neutrophils isolated from anticoagulated blood and labelled with membrane dye (CellMask DeepRed) were perfused in the presence of DyLight 550 (DL550) conjugated KIM127 and DyLight 488 (DL488) conjugated mAb24 at 6 dyn cm<sup>-2</sup> and imaged with a newly developed triple-colour qDF (TqDF) setup. Smart segmentation image processing (Supplementary Fig. 4) was used to remove background and generate binary images of the neutrophil footprint in contact with the substrate (Fig. 1a,b) from raw images (Supplementary Fig. 5a) and reproduce the cluster morphology with better signal-to-noise ratio (Supplementary Fig. 5b). On the P-selectin/ICAM-1/IL-8 substrate, neutrophils rolled and arrested (Fig. 1c). Unlike the nearly homogeneous distribution of total  $\alpha_L\beta_2$  integrins on the cell surface, both KIM127<sup>+</sup> and mAb24<sup>+</sup>  $\beta_2$  integrins were present in small clusters (Fig. 1d-f, Supplementary Figs 4 and 5 and Supplementary Movie 1) before arrest (time = 0 s) and remained in clusters of similar size (Supplementary Fig. 6) after arrest. In the overlaid images (Fig. 1f and Supplementary Movie 1),  $E^+H^-$  (KIM127<sup>+</sup>mAb24<sup>-</sup>, red) and  $E^+H^+$  (KIM127<sup>+</sup>mAb24<sup>+</sup>, yellow)  $\beta_2$  integrins were observed during neutrophil rolling and arrest as expected. Unexpectedly, neutrophils also showed clusters of mAb24<sup>+</sup>KIM127<sup>-</sup>  $\beta_2$  integrins ( $E^-H^+$ , green). Very few clusters of mAb24<sup>+</sup>KIM127<sup>+</sup> integrins ( $E^+H^+$ , yellow, time before arrest) are observed in rolling neutrophils before arrest. Dye switch experiments excluded nonspecific effects of the fluorochromes used (Supplementary Fig. 7a). These experiments show that neutrophils rolling on 'complete' substrate (P-selectin/ICAM-1/IL-8) show the complete physiologic transition from rolling to arrest within ~30 s (Fig. 2a) and express small (~0.1  $\mu\text{m}^2$ ) clusters of  $E^+H^-$ ,  $E^-H^+$  and  $E^+H^+$   $\beta_2$  integrins.

**Different roles of P-selectin and IL-8.** To assess which component on the substrate induces integrin activation, we tested

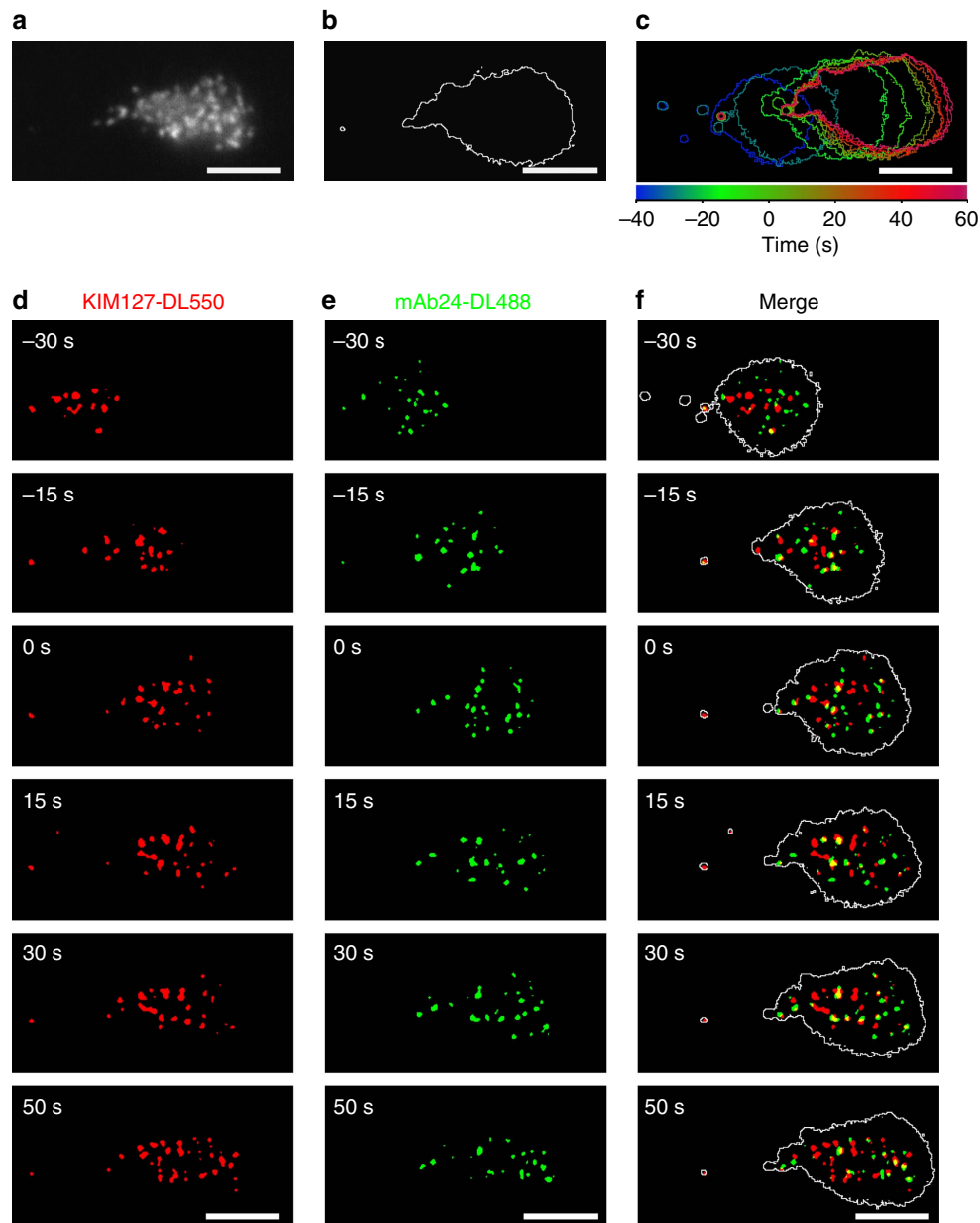


**Figure 1 |  $\beta_2$  integrin  $E^+$  and  $H^+$  conformations on human neutrophil footprint.** (a) A typical image of fluorescently labelled neutrophil membrane. (b) Footprint outline of a neutrophil generated from membrane fluorescence in a. (c) Footprint outlines of a typical cell during rolling on the P-selectin/ICAM-1/IL-8 substrate at a wall shear stress of  $6 \text{ dyn cm}^{-2}$  (arrest at time = 0 s); time was coded in rainbow colours as shown in colour bar. (d-f)  $E^+$   $\beta_2$  integrins identified by KIM127-DL550 (red in d and f), and  $H^+$  by mAb24-DL488 (green in e and f) during neutrophil rolling on P-selectin/ICAM-1/IL-8 substrate. Footprint outlines shown in white in f. Binary images generated by smart segmentation;  $E^+H^+$ ,  $E^+H^-$  and  $E^-H^+$  clusters appear yellow, red and green, respectively, in f; scale bars,  $5 \mu\text{m}$ .

neutrophil rolling and adhesion on ‘incomplete’ substrates: P-selectin only, P-selectin/ICAM-1 and P-selectin/IL-8 (Fig. 2). On the ‘complete’ P-selectin/ICAM-1/IL-8 substrate, neutrophils rolled at a velocity of  $\sim 1.0 \mu\text{m s}^{-1}$  (Fig. 2a) before arrest at time = 0. As expected<sup>34</sup>, neutrophils rolled much faster ( $\sim 3.1 \mu\text{m s}^{-1}$ ) on P-selectin only (Fig. 2b), whereas the P-selectin/ICAM-1 substrate (Fig. 2c) supported slow rolling ( $\sim 1.2 \mu\text{m s}^{-1}$ ), but no arrest. Adding IL-8 to the P-selectin substrate (Fig. 2d) did not reduce rolling velocity ( $\sim 3.1 \mu\text{m s}^{-1}$ ) and did not support arrest. Quantitative analysis of the cluster number (Fig. 2e) showed that neutrophils rolling on P-selectin/ICAM-1/IL-8 substrate started with  $\sim 9 E^+H^-$ ,  $\sim 9 E^-H^+$  and  $\sim 3 E^+H^+$  clusters at  $-30 \text{ s}$ . As the cells continued rolling,

the number of  $E^+H^+$  clusters increased and reached  $9 \pm 1$  when the cells arrested (time = 0 s, Fig. 2e and Supplementary Fig. 6a). The step change from pre-arrest to arrest was highly significant (Fig. 2f). The number of  $E^+H^-$  clusters (Fig. 2g) and  $E^-H^+$  clusters (Fig. 2h) also significantly increased upon arrest. The total area of  $E^+H^-$ ,  $E^-H^+$  and  $E^+H^+$  clusters increased in proportion to the cluster number (Supplementary Fig. 6b) and the size of each cluster did not change significantly (Supplementary Fig. 6c).

When neutrophils were rolling on P-selectin only (Fig. 2i-l),  $E^+H^-$  clusters were induced (red, Fig. 2i,k), as expected<sup>33,34</sup>, but no  $E^+H^+$  clusters (yellow, Fig. 2i,j) or  $E^-H^+$  clusters (green, Fig. 2i,l) were observed. Induction of  $E^+H^-$  clusters but not

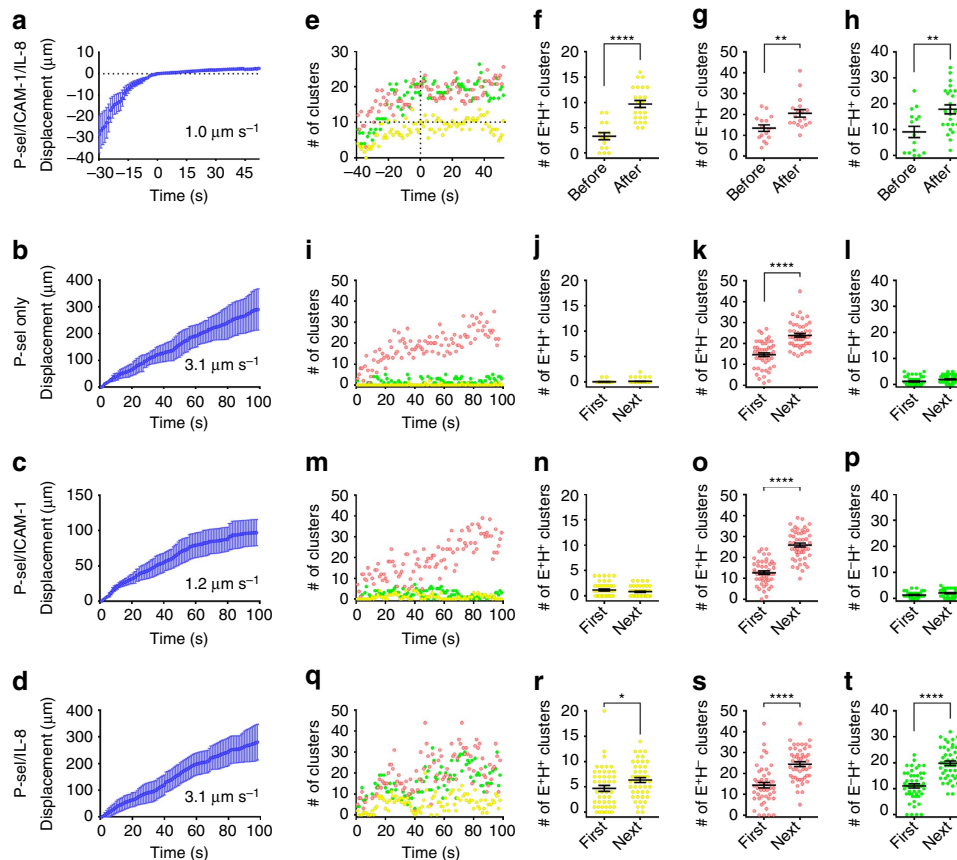


**Figure 2 | Differential effects of ICAM-1 and IL-8 on integrin activation in human neutrophils.** (a–d) Displacements of typical cells ( $n = 9$ , mean  $\pm$  s.e.m.) during rolling on P-selectin/ICAM-1/IL-8 (a, arrest at time = 0 s), P-selectin only (b), P-selectin/ICAM-1 (c) or P-selectin/IL-8 (d) substrates, respectively. Average rolling velocity (for a: before arrest) determined from linear regression. (e) Dynamics of cluster number per cell ( $E^+H^-$  red,  $E^-H^+$  green,  $E^+H^+$  yellow) rolling on P-selectin/ICAM-1/IL-8. (f–h) Number of  $E^+H^+$  (f),  $E^-H^+$  (g) or  $E^+H^-$  (h) clusters averaged before (–30 and –15 s,  $n = 16$ ) and after (0, 15 and 30 s,  $n = 24$ ) arrest in eight cells rolling on P-selectin/ICAM-1/IL-8; each time point of each cell represented by one dot, mean  $\pm$  s.e.m.  $**P < 0.01$ ,  $****P < 0.0001$ . (i–t)  $E^+H^-$  (red),  $E^-H^+$  (green) and  $E^+H^+$  (yellow) clusters for neutrophils rolling on P-selectin only (i), P-selectin/ICAM-1 (m), and P-selectin/IL-8 (q) coated substrates.  $E^+H^+$  (j,n,r),  $E^-H^+$  (k,o,s) and  $E^+H^-$  (l,p,t) clusters in the footprint of cells rolling on P-selectin only (j–l), P-selectin/ICAM-1 (n–p) or P-selectin/IL-8 (r–t) in the first 50 s (first) and the next  $\sim 50$  s (next) of rolling. Mean values and s.e.ms (error bars) were presented.  $*P < 0.05$ ,  $****P < 0.0001$  in unpaired student *t*-test.

$E^-H^+$  or  $E^+H^+$  clusters was highly significant when comparing the first 50 s and the next  $\sim 50$  s of rolling (Fig. 2j–l). Rolling neutrophils on P-selectin/ICAM-1 substrate (no chemokine, Fig. 2m–p) produced a similar increase in  $E^+H^-$  integrin (red, Fig. 2m,o) as on P-selectin. As expected, the cells rolled more slowly because the  $E^+H^-$  integrin was able to bind to ICAM-1 with intermediate affinity. Neither  $E^+H^+$  integrin (yellow, Fig. 2m,n) nor  $E^-H^+$  integrin (green, Fig. 2m,p) were observed. This changed drastically when chemokine was available on the P-selectin/IL-8 substrate (no ICAM-1, Fig. 2q–t). Strikingly,  $E^+H^+$  clusters (yellow, Fig. 2r) and  $E^-H^+$  clusters (green, Fig. 2t) were induced along with the expected  $E^+H^-$  clusters (red, Fig. 2s). Taken together, these data suggest that P-selectin binding is sufficient to induce integrin extension and chemokine is necessary to induce headpiece-opening.

#### $E^+H^+$ clusters derived from both $E^+H^-$ and $E^-H^+$ clusters.

The strong dependence of arrest on the appearance of  $\sim 9$   $E^+H^+$  clusters (Fig. 2e and Supplementary Fig. 6a) suggests that  $E^+H^+$  integrins are the functional entity for binding ICAM-1 in trans. When focusing on individual clusters labelled with KIM127-DL550 or mAb24-DL488, we observed that both  $E^+H^-$  integrins (red)

and  $E^-H^+$  integrins (green) transitioned to  $E^+H^+$  (yellow, Fig. 3a). Dye switch experiments excluded nonspecific effects of the fluorochromes used (Supplementary Fig. 7b). About one-third of  $E^+H^-$  clusters became  $E^+H^+$  within 4 s (Fig. 3b,c,  $n = 15$ ).  $E^-H^+$  clusters also became  $E^+H^+$  at a similar rate (Fig. 3d,e,  $n = 15$ ). When tracking the history of the clusters on arrested cells, many  $E^-H^+$  and  $E^+H^-$  clusters remained  $E^-H^+$  or  $E^+H^-$ , respectively, but some clusters ( $\sim 5$  per neutrophil) converted from  $E^+H^-$  or  $E^-H^+$  to  $E^+H^+$  (Fig. 3f). This was caused by an increase in the number of double positive (red and green) pixels over time and independent of small random fluctuations in background intensity (Supplementary Fig. 8). These findings suggest a new alternative pathway (Supplementary Fig. 1b) in which integrin undergoes a conformational change from  $E^-H^-$  to  $E^-H^+$  first and then to  $E^+H^+$ , clearly different from the canonical pathway suggested by the switchblade model. These two pathways both contributed to fully activated ( $E^+H^+$ ) integrins on neutrophils during transition from rolling to arrest on P-selectin/ICAM-1/IL-8 substrate.

**Three-dimensional localization of integrin activation.**  $E^+H^+$  integrins can bind ligand in trans with high affinity. The  $E^+H^+$  conformation is a necessary, but not sufficient condition for

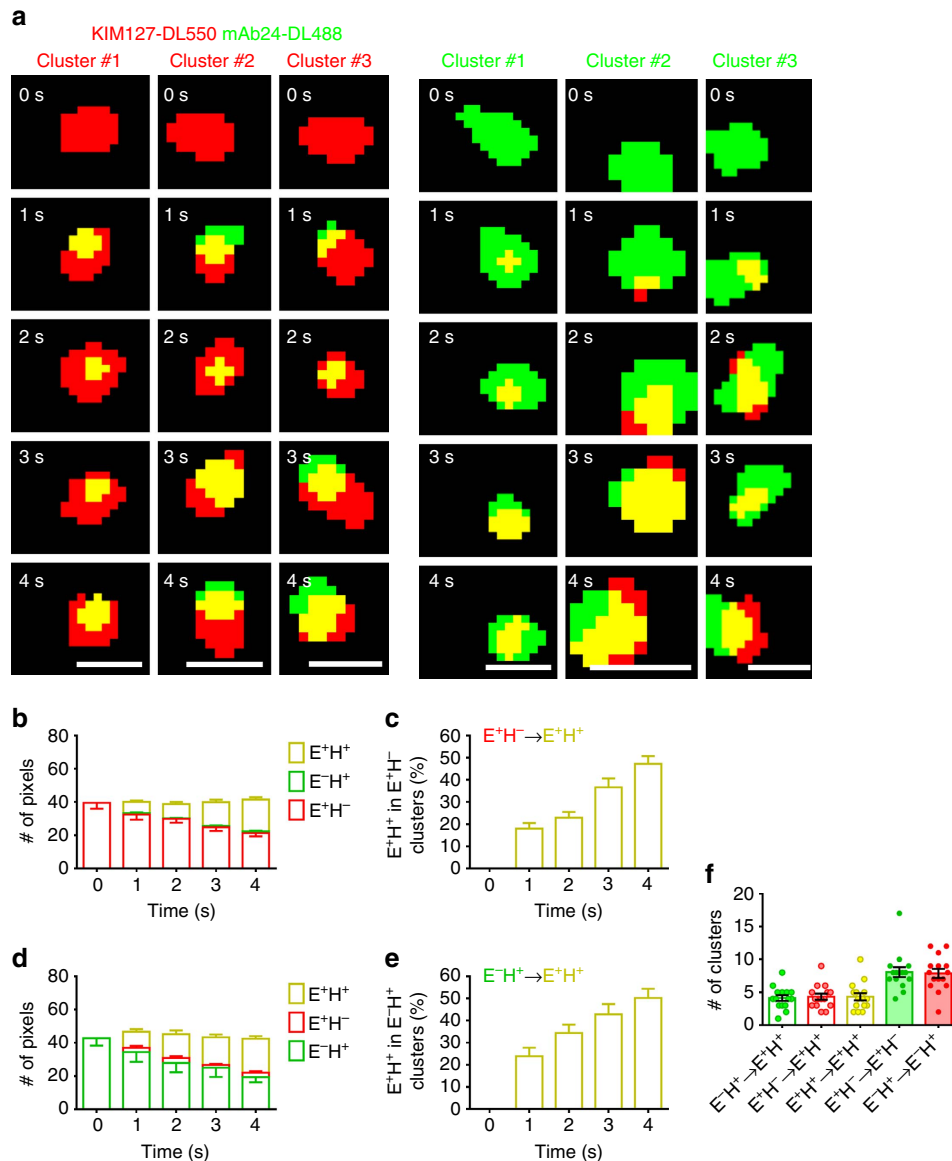


**Figure 3 | Two pathways of conformational transitions during  $\beta_2$  integrin activation.** (a) Three examples of KIM127-DL550 (red,  $E^+H^-$ ) or mAb24-DL488 (green,  $E^-H^+$ ) clusters transitioning to  $E^+H^+$  (yellow) over 4 s in the footprint of primary human neutrophils rolling on P-selectin, ICAM-1 and IL-8; scale bars, 0.5  $\mu\text{m}$ . (b–e) Mean values of pixel numbers per cluster in colours as indicated (b,d) and percentage of  $E^+H^+$  pixels (c,e) of 15 clusters starting as  $E^+H^-$  (b,c) or 15 clusters starting as  $E^-H^+$  (d,e); s.e.m.s were shown as error bars. Data collected from static cells (pre-arrest and arrested). (f) Transition history of the clusters on arrested cells ( $n=15$ , one dot per cell). Mean values and s.e.m.s (error bars) were presented.

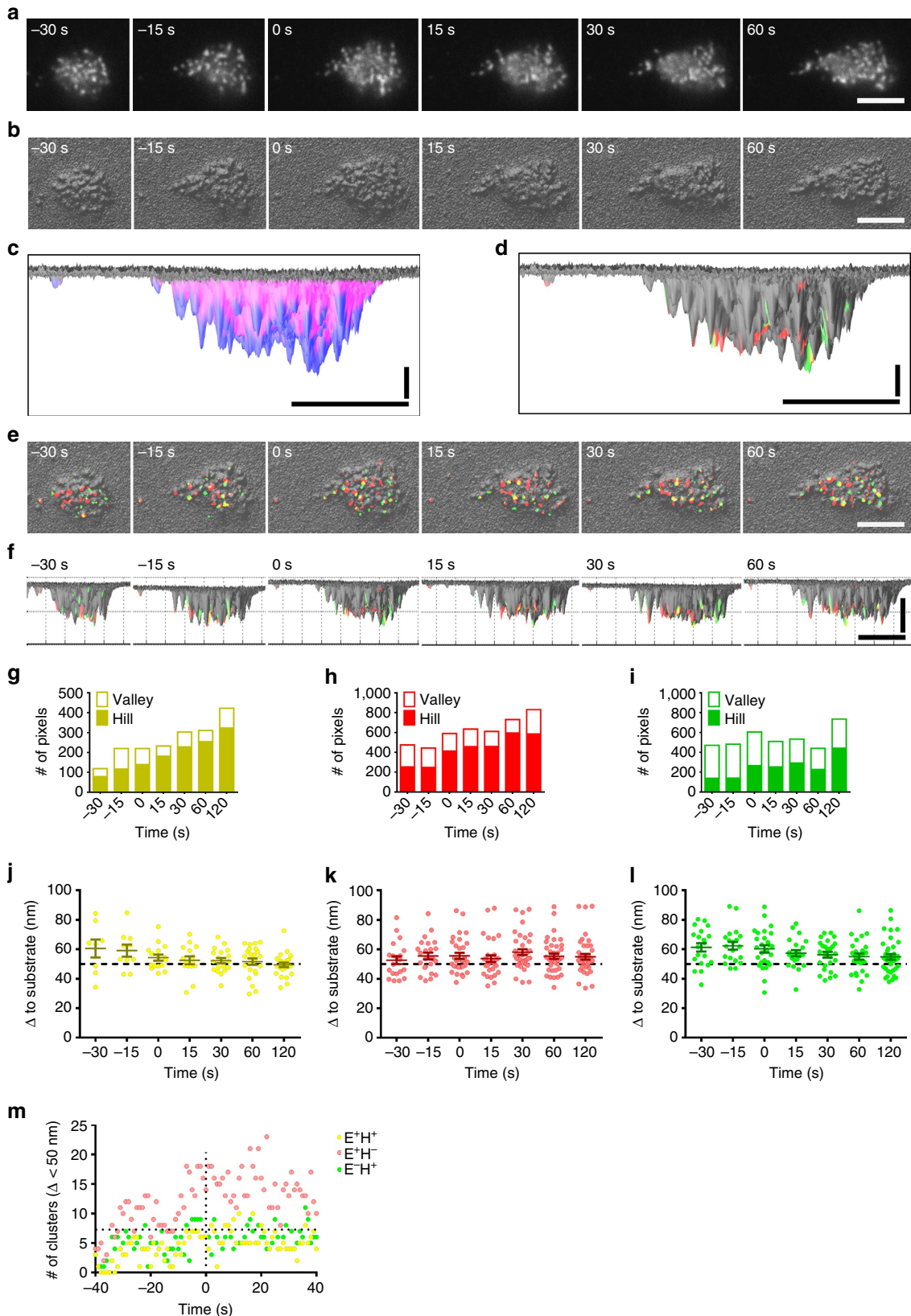
binding, since the ligand-binding I domain of  $\alpha_L$  or  $\alpha_M$  is only about 23 nm<sup>42</sup> above the plasma membrane when extended. The extended  $\beta_2$  integrin-ICAM-1-assembly is about 42 nm long<sup>43</sup>. Neutrophils have microvilli that are  $\sim 200$  nm high<sup>44</sup>, and  $\beta_2$  integrins are known to be located both on microvilli (hills) and in the ‘valleys’ between microvilli<sup>45</sup>. For  $E^+H^+$   $\beta_2$  integrins to reach ligand in trans, they effectively need to be near the top of the microvilli. To test what fraction of integrin clusters met these criteria, we converted<sup>15</sup> the raw membrane data (Fig. 4a) into 3D footprints (Fig. 4b). Automated smart segmentation showed  $27 \pm 1\%$  hills and  $73 \pm 1\%$  valleys (Fig. 4c and Supplementary Fig. 9). Next, we superimposed  $E^+H^+$  (yellow),  $E^+H^-$  (red) and  $E^-H^+$  (green) integrin clusters (Fig. 4d,e) on the 3D topography. Rotation by 90 degrees (Fig. 4d,f and Supplementary Movie 2) allowed us to map all clusters within  $\sim 100$  nm from the surface. Interestingly, significantly more ( $P < 0.05$ ) of the  $E^+H^+$

(Fig. 4g,  $70 \pm 4\%$ ) and  $E^+H^-$  (Fig. 4h,  $68 \pm 4\%$ ) clusters were on hills and thus close to the substrate than  $E^-H^+$  clusters (Fig. 4i). The fraction of  $E^+H^+$  and  $E^+H^-$  integrin on hills significantly increased with time of rolling and continued to increase after arrest (time = 0 s).

Integrin can bind ICAM-1 on the substrate only when the integrin is within  $\sim 50$  nm from the substrate (Supplementary Fig. 10). Analyzing the number of  $E^+H^-$ ,  $E^+H^+$  and  $E^-H^+$  clusters within 50 nm of the substrate shows that during rolling, about three  $E^+H^+$  clusters are ‘within reach’, and the number of  $E^+H^+$  clusters close to the substrate (Fig. 4j, yellow) continues to increase until arrest. The number of  $E^+H^-$  clusters (Fig. 4k, red) within 50 nm of the substrate also increases during rolling. Some  $E^-H^+$  clusters (Fig. 4l, green) are also within 50 nm, but this is irrelevant to ligand binding, because the bent conformation is not expected to bind ligand in trans even if the headpiece is

‘open’ (Supplementary Fig. 10). The dynamics of integrin conformations within 50 nm to the substrate over time of rolling and arrest is shown in Fig. 4m, which shows that arrest is triggered by  $\sim 7$   $E^+H^+$  clusters that are close enough to the substrate to bind ICAM-1 in trans.

To directly measure the number of fully activated  $E^+H^+$   $\beta_2$  integrins that are needed for arrest, we measured the sites of KIM127 and mAb24 on the neutrophil surface by calibration beads with known antibody-binding sites using flow cytometry. Calculating from the fluorescence intensity integral of  $E^+H^+$



clusters at the time of arrest ( $t = 0$ ), we find that  $258 \pm 41 E^+H^+$  integrin molecules are present in the neutrophil footprint at the time of arrest.

**$E^-H^+$   $\beta_2$  integrins bind ICAM-1 on neutrophils in *cis*.** The discovery of  $E^-H^+$   $\beta_2$  integrins on human neutrophils is the first report of  $E^-H^+$  integrins on any physiological relevant cell. We reasoned that such bent high-affinity integrins may have a specific function. Since  $E^-H^+$  integrin is not expected to bind ligand in *trans*, we considered whether  $E^-H^+$  integrin may bind ligand in *cis*, that is, ICAM-1 expressed on the neutrophil. Human LFA-1 and Mac-1 bind domain 1 (ref. 46) and domain 3 (ref. 47) of human ICAM-1, respectively. To directly test whether  $E^-H^+$  LFA-1 and Mac-1 could bind ICAM-1 in *cis* (on the neutrophil), we conducted Förster resonance energy transfer (FRET) experiments that report proximity of molecules within 1–10 nm (Fig. 5). When FRET occurs, emission at the shorter wavelength donor fluorochrome (for example, fluorescein isothiocyanate, FITC) is reduced (quenching at 525/50 nm), because some energy is transferred to the higher wavelength acceptor fluorochrome (for example, DL550). Conversely, FRET increases the emission of the higher wavelength fluorochrome (for example, DL550, measured at 575/25 nm). We reasoned that FRET should occur between mAb24 (binding  $\beta_2 H^+$ ) and ICAM-1 domain 1 detected by mAb HA58 (Fig. 5a). Since mAb HA58 is function-blocking<sup>48</sup> (disables ICAM-1 domain 1 binding to LFA-1), this assay directly tests the interaction of Mac-1 with domain 3 of ICAM-1. We indeed observed a significant decrease in donor fluorescence (Fig. 5b) and significant increase in acceptor fluorescence (Fig. 5c). This was specific, because FRET quenching did not occur when the acceptor mAb24-DL550 was absent or replaced by an isotype control antibody or KIM127-DL550, or when Mac-1 binding to ICAM-1 was blocked by mAb R6.5 (Fig. 5d)<sup>49</sup>. Similarly, the gain of acceptor fluorescence was blocked by adding R6.5, or when an irrelevant donor was used (anti-CD14-FITC, or isotype control, Fig. 5e) instead of HA58-FITC. Based on the FRET efficiency as measured, the average distance between the  $\beta_2$  I-like domain (mAb24-binding site) and ICAM-1 domain 1 (HA58-binding site) is calculated to be  $\sim 9.9$  nm, which is consistent with the known molecular dimensions.

Having shown that  $E^-H^+$  neutrophil  $\beta_2$  integrins directly bind ICAM-1 in *cis*, we reasoned that this binding may stabilize  $E^-H^+$  clusters. Thus,  $E^-H^+$  clusters should be decreased when ICAM-1 binding to LFA-1 (using mAb HA58) and Mac-1 (using mAb R6.5) were blocked (Fig. 6a). Indeed, blocking ICAM-1 binding in *cis* (ICAM-1 blk) reduced the number of  $E^-H^+$  clusters (Fig. 6b,c) at the time of neutrophil arrest (0 s). We found no significant difference in  $E^+H^+$  (Fig. 6d) or  $E^+H^-$  (Fig. 6e) clusters when ICAM-1 was blocked on the neutrophils, but ICAM-1 blk neutrophils reach the number of  $E^+H^+$  clusters needed for arrest faster. Under control conditions, the number of

$E^-H^+$  clusters increased with time, and this did not happen when ICAM-1 was blocked (Fig. 6f). If indeed  $\beta_2$  integrin interaction with ICAM-1 in *cis* stabilized the  $E^-H^+$  conformation, then the duration of  $E^-H^+$  clusters (time before having  $E^+H^+$  on the cluster) should be reduced. Indeed, the average duration of  $E^-H^+$  clusters was reduced from  $>5$  s to  $<2$  s (Fig. 6g,h).

**$E^-H^+$   $\beta_2$  integrins inhibit neutrophil adhesion.** Since  $\beta_2$  integrin interaction with ICAM-1 in *cis* stabilized the  $E^-H^+$  conformation, we hypothesized that this may represent an auto-inhibitory pathway, because  $E^-H^+$  integrins are not available for ligand binding in *trans* and thus are not expected to support cell adhesion under flow. Indeed, when ICAM-1 was blocked, human neutrophils arrested much quicker and rolled for a shorter distance than untreated human neutrophils on P-selectin/ICAM-1/IL-8 substrate (Fig. 7a,b). Human neutrophils express ICAM-1, a ligand for LFA-1 and Mac-1, and ICAM-3, a ligand for LFA-1, but not ICAM-2 (Supplementary Fig. 11). Therefore, we tested the rolling duration and distance (until arrest, Fig. 7c,d, respectively), the rolling velocity (Fig. 7e) and the resulting number of arrested neutrophils (Fig. 7f) with or without ICAM-1 and/or ICAM-3 blockade. Blocking ICAM-1 domain 1 (the LFA-1-binding site) was sufficient to make neutrophils adhere significantly faster (shorter rolling duration), resulting in more arrested neutrophils. Blocking both LFA-1 and Mac-1-binding sites on ICAM-1 further accelerated neutrophil accumulation. The effect of blocking ICAM-1 was similar to the effect of blocking ICAM-3, and blocking both ICAM-1 and ICAM-3 further reduced rolling duration, distance and velocity and further increased the number of arrested neutrophils.

To specifically look at the contributions of LFA-1 and Mac-1, we blocked Mac-1 by mAb ICRF44 (Fig. 7g–j) or LFA-1 by mAb TS1/22 (Fig. 7k–n). Since LFA-1 binds both ICAM-1 and ICAM-3, we tested the contribution of both ligands and found that blocking ICAM-3 alone had a stronger effect on the number of arrested neutrophils than blocking ICAM-1 alone. This is consistent with the higher expression of ICAM-3 than ICAM-1 on human neutrophils (Supplementary Fig. 11). We conclude that ICAM-3 is the dominant LFA-1 ligand in *cis*. Since Mac-1 binds only to ICAM-1, we tested its contribution by blocking the Mac-1 binding to ICAM-1 using mAb R6.5 (ref. 49). This intervention significantly decreased rolling duration, distance and velocity and significantly increased Mac-1-dependent neutrophil arrest. These data show that Mac-1 interaction with ICAM-1 in *cis* significantly contributes to limiting neutrophil accumulation.

To directly address the *in vivo* relevance of our findings, we performed *in vivo* mouse experiments. ICAM-1 and 2 are both expressed on mouse neutrophils<sup>16,50</sup>. We performed *in vivo* cremaster imaging on mice reconstituted with mixed ICAM-1/2-double-knockout<sup>51,52</sup> and DsRed-wild type (1:1) bone marrow. ICAM-1/2-double-knockout leukocytes

**Figure 4 | 3D distributions of  $\beta_2$  integrin activation clusters in primary human neutrophils.** (a) Neutrophil membrane (CellMask DeepRed) before and after arrest (0 s) of one representative neutrophil rolling on P-selectin, ICAM-1 and IL-8. (b) Membrane signal converted to hills (microvilli) and valleys (space between microvilli). (c,d) Hills (blue) and valleys (magenta) segmented (c) or  $E^+H^-$  (red),  $E^-H^+$  (green) or  $E^+H^+$  (yellow) clusters (d) were identified at time of arrest (0 s). (e,f) Top-view (e) and side-view (f) of the 3D topography overlaid with  $E^+H^-$  (red),  $E^-H^+$  (green) or  $E^+H^+$  (yellow) clusters; binary images. Horizontal scale bars, 5  $\mu$ m, vertical scale bar, 20 nm for d, scale bar, 50 nm for f. (g–i) Most  $E^+H^+$  (g,  $70 \pm 4\%$ ) and  $E^+H^-$  (h,  $68 \pm 4\%$ ) cluster pixels were on hills. Most  $E^-H^+$  cluster pixels (i,  $71 \pm 0\%$ ) were in valleys before arrest ( $P < 0.01$  and  $P < 0.05$  compared with  $E^+H^-$  and  $E^+H^+$  cluster pixels in unpaired student *t*-test, respectively) and more  $E^-H^+$  cluster pixels ( $52 \pm 6\%$ ) localized to the hills after arrest ( $P < 0.05$  and  $P < 0.01$  compared with  $E^+H^-$  and  $E^+H^+$  cluster pixels in unpaired student *t*-test, respectively). The  $E^+H^+$  (g),  $E^+H^-$  (h) and  $E^-H^+$  (i) cluster pixels on the hills increased with time (the slopes were significantly non-zero, *F*-test,  $P < 0.01$ ). (j–l) Distance ( $\Delta$ ) of  $E^+H^+$  (yellow, j),  $E^+H^-$  (red, k) or  $E^-H^+$  (green, l) integrin clusters to the substrate. The dashed line at 50 nm separates the integrin clusters within reach ( $\leq 50$  nm) from those beyond reach ( $> 50$  nm). Each cluster represented by one dot, mean values and s.e.ms (error bars) were presented. (m) Number of clusters within 50 nm to the substrate per cell ( $E^+H^-$  red,  $E^-H^+$  green,  $E^+H^+$  yellow) during rolling on the substrate of P-selectin/ICAM-1/IL-8 (arrest at 0 s).

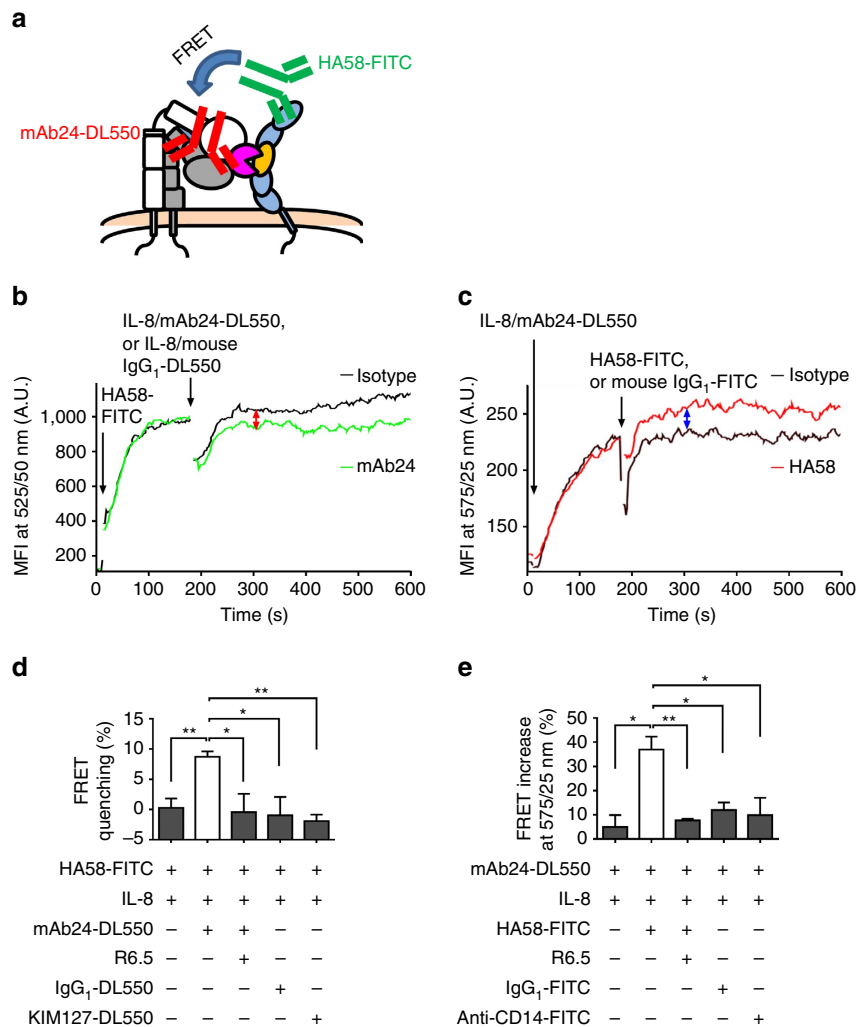


**Figure 5 | E<sup>-</sup>H<sup>+</sup> Mac-1 binds ICAM-1 in cis.** (a) Schematic of assessing the *cis* interaction between E<sup>-</sup>H<sup>+</sup> Mac-1 and neutrophil ICAM-1 by FRET between ICAM-1 domain 1 (HA58-FITC, donor) and H<sup>+</sup> integrin (mAb24-DL550, acceptor). (b,c) Donor fluorescence decrease (green in b) and acceptor fluorescence increase (red in c) shows FRET of HA58-FITC with mAb24-DL550, but not with isotype controls (IgG<sub>1</sub>-DL550 as acceptor, black in b; and IgG<sub>1</sub>-FITC as donor, black in c). (d,e) Donor fluorescence decrease (d) and acceptor fluorescence increase (e) of HA58-FITC-mAb24-DL550 pairs and controls measured at 2–3 min after adding IL-8 and acceptor or donor, respectively. Blocking of E<sup>-</sup>H<sup>+</sup> Mac-1-ICAM-1 interactions (mAb R6.5) eliminated the donor fluorescence decrease and acceptor fluorescence increase.  $n = 3$ , mean values and s.e.m.s (error bars) were presented. \*  $P < 0.05$ , \*\*  $P < 0.01$  in unpaired student *t*-test. A.U., arbitrary unit.

(non-fluorescent) showed significantly decreased rolling velocity in cremaster venules (Fig. 7o). After injecting the chemokine CXCL1, the number of arrested ICAM-1/2-double-knockout leukocytes was twice that of wild-type neutrophils (Fig. 7p). These data show that the binding of E<sup>-</sup>H<sup>+</sup>  $\beta_2$  integrin to ICAM-1 and 2 in *cis* strongly inhibits leukocyte adhesion *in vivo*.

Based on the finding that integrin activation blockade by interaction of E<sup>-</sup>H<sup>+</sup>  $\beta_2$  integrins with ICAMs in *cis* is relevant *in vitro* and *in vivo*, we asked whether it would also limit neutrophil aggregation. To test this, we performed an aggregation assay (Supplementary Fig. 12), where we stained human neutrophils with two different dyes (carboxyfluorescein succinimidyl ester (CFSE) and cell tracker orange (CMRA)) and tested the aggregation between the two populations. When ICAMs were blocked on the CMRA population, thus effectively blocking the *cis* interaction and liberating  $\beta_2$  integrins, the percentage of heteroaggregates increased about threefold. When we further blocked  $\beta_2$  integrins on the other (CFSE) population, which released the *cis*-binding ICAMs, CFSE-CMRA aggregates increased by a further factor of two. Therefore, without the

inhibition of integrin extension by binding ICAMs in *cis*, neutrophil aggregation would be expected to be sixfold higher than it actually is. These results directly demonstrate that the *cis* interaction between E<sup>-</sup>H<sup>+</sup>  $\beta_2$  integrin and ICAMs provides a relevant mechanism that inhibits neutrophil aggregation in suspension.

Taken together, our data support a new model (Supplementary Fig. 1b) where resting E<sup>-</sup>H<sup>-</sup> LFA-1 and Mac-1 are stimulated by chemokine to assume the E<sup>-</sup>H<sup>+</sup> conformation that binds mAb24, but not KIM127. This conformation is stabilized by interaction with ICAM-1 on the neutrophil in *cis*. When extension occurs, this converts E<sup>-</sup>H<sup>+</sup> to E<sup>+</sup>H<sup>+</sup> integrin, which is now able to bind ICAM-1 in *trans* (on the substrate, endothelium or other leukocytes) and thus promote arrest.

## Discussion

Here we elucidate the molecular mechanism of  $\beta_2$  integrin-dependent neutrophil arrest. As expected, rolling neutrophils express some  $\beta_2$  integrins in the E<sup>+</sup>H<sup>-</sup> conformation.

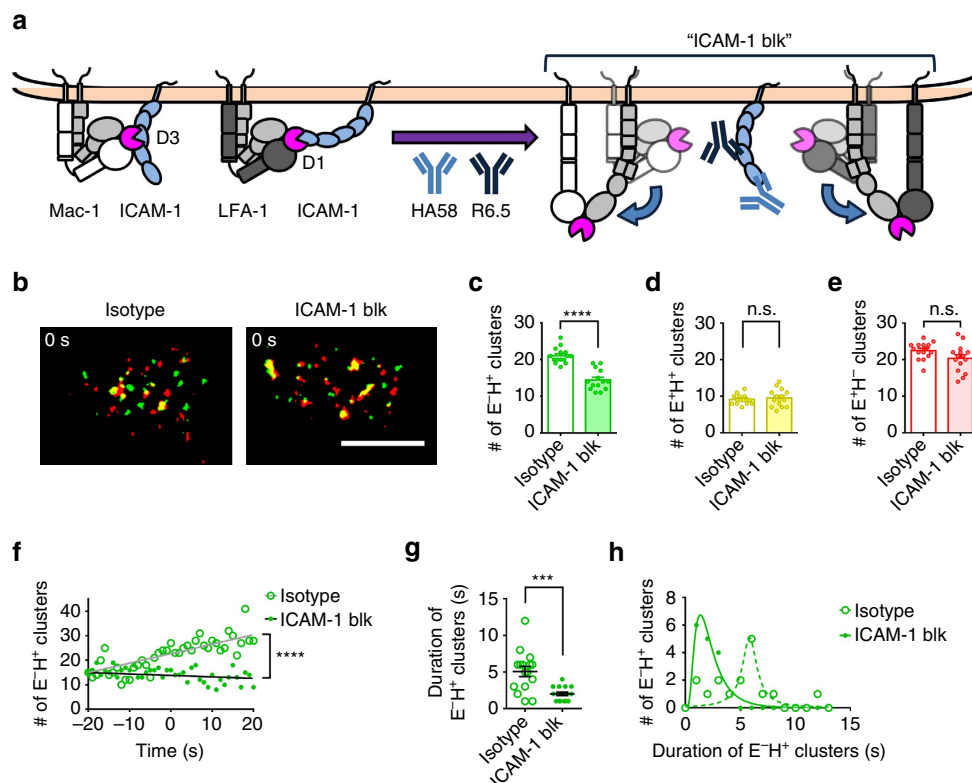


**Figure 6 | Blocking  $E^-H^+$  integrin binding to neutrophil ICAM-1 promotes its transition to  $E^+H^+$ .** (a) Schematic showing the hypothesis that the *cis* interactions of  $E^-H^+$  integrin (both LFA-1 and Mac-1) and neutrophil ICAM-1 may stabilize the  $E^-H^+$  integrin. (b) Integrin clusters ( $E^-H^+$  red,  $E^+H^+$  green,  $E^+H^+$  yellow) on arresting neutrophils rolling on P-selectin/ICAM-1/IL-8 with or without neutrophil ICAM-1 blocking by mAbs HA58 and R6.5; scale bar, 5  $\mu\text{m}$ . (c–e) ICAM-1 blocking decreased the number of  $E^-H^+$  clusters at arrest (c,  $n = 15$  cells). The number of  $E^+H^+$  (d,  $n = 15$  cells) and  $E^-H^+$  clusters (e,  $n = 15$  cells) at arrest with or without ICAM-1 blocking. (f) Dynamics of  $E^-H^+$  clusters with or without ICAM-1 blockade on cells rolling on P-selectin/ICAM-1/IL-8. (g,h) ICAM-1 blocking decreased the duration of  $E^-H^+$  clusters before transitioning to  $E^+H^+$  clusters (g,  $n = 16$  clusters). Duration histograms (h, bin = 1 s). Mean values and s.e.m.s (error bars) were presented in (c–e) and (g). Log Gaussian (ICAM-1 blk) and Lorentzian (isotype) fits were used in h. n.s.  $P > 0.05$ , \*\*  $P < 0.01$ , \*\*\*  $P < 0.001$ , \*\*\*\*  $P < 0.0001$  in unpaired student *t*-test. n.s., not significant.

Unexpectedly, the  $E^-H^+$  integrins are organized in clusters with an average size of  $\sim 25$  pixels ( $\sim 0.1 \mu\text{m}^2$ ). Unlike bulk  $\beta_2$  integrins, most of these  $E^-H^+$  clusters are on the tips of microvilli and thus able to reach ICAM-1 on the flat substrate. *In vivo*, neutrophil hills and valleys may interdigitate with endothelial hills and valleys, but this cannot be imaged with sufficient resolution by intravital microscopy. Very few clusters of high-affinity ( $E^+H^+$ ) integrin are observed on rolling neutrophils. When immobilized chemokine is added, both  $E^-H^+$  and  $E^+H^+$  clusters are induced. When the number of  $E^+H^+$  clusters reaches  $\sim 9$  ( $\sim 7$  within 50 nm from substrate), the cell stops rolling and arrests. We estimate that 258 fully activated  $E^+H^+$   $\beta_2$  integrin molecules are sufficient to arrest a human neutrophil at  $6 \text{ dyn cm}^{-2}$ .

According to the switchblade model<sup>23,25</sup> of integrin activation,  $E^+$  precedes  $H^+$ . Thus, the appearance of  $E^-H^+$  clusters was completely unexpected. The  $E^-H^+$  conformation was suggested by an electron microscopic image of  $\alpha_V\beta_3$  integrin<sup>53</sup>, a crystal structure of  $\alpha_X\beta_2$  stabilized by introduced disulfide bridges<sup>54</sup>, and three Mac-1 mutants<sup>55</sup>. However, these first two constructs lacked transmembrane and cytoplasmic domains and the third introduced physiologically irrelevant mutations. Thus, the physiological significance remained unclear. Here we show that the  $E^-H^+$  integrin conformation exists on primary human cells. Our findings suggest that integrin  $H^+$  and  $E^+$  are regulated individually, which disagrees with the canonical switchblade model<sup>25</sup>, where integrin  $H^+$  requires integrin extension ( $E^+$ ).

We show that PSGL-1 signalling is sufficient to induce  $E^+$ , whereas chemokine signalling necessary for  $H^+$ .

Beyond these results that are relevant to our understanding of basic integrin biology, we discovered that  $E^-H^+$  integrins bind ICAMs in *cis*, which effectively inhibits cell adhesion as evidenced by prolonged rolling distance, prolonged rolling time and reduced number of adherent neutrophils. This is a new, powerful and unexpected endogenous anti-inflammatory mechanism that impacts inflammation and immunity. This new mechanism not only limits neutrophil adhesion under flow, but also curbs neutrophil aggregation, which is associated with acute lung injury<sup>56</sup>, sepsis<sup>57</sup> and coronary artery disease<sup>58</sup>.  $E^-H^+$  LFA-1 binds to both ICAM-1 and ICAM-3 in *cis*;  $E^-H^+$  Mac-1 binds to ICAM-1 in *cis*. Thus, both major  $\beta_2$  integrins on neutrophils are inhibited by binding ICAMs in *cis*. The FRET assay provides direct evidence of close proximity between  $H^+E^-$   $\beta_2$  integrins and ICAMs. The functional data (adhesion and aggregation assays) are consistent with our interpretation. Direct evidence to demonstrate the existence of the *cis* interaction of the  $\beta_2$  integrins with ICAMs might ultimately be provided by co-crystallization.

It is known that Mac-1 on neutrophils is increased upon chemokine stimulation by degranulation<sup>33</sup>. However, the degranulation does not occur until  $\sim 5$  min after chemokine. In our investigation, we considered the conformational changes of  $\beta_2$  integrins only less than 1 min after exposure to IL-8. Thus, Mac-1 degranulation does not influence our findings. Whether

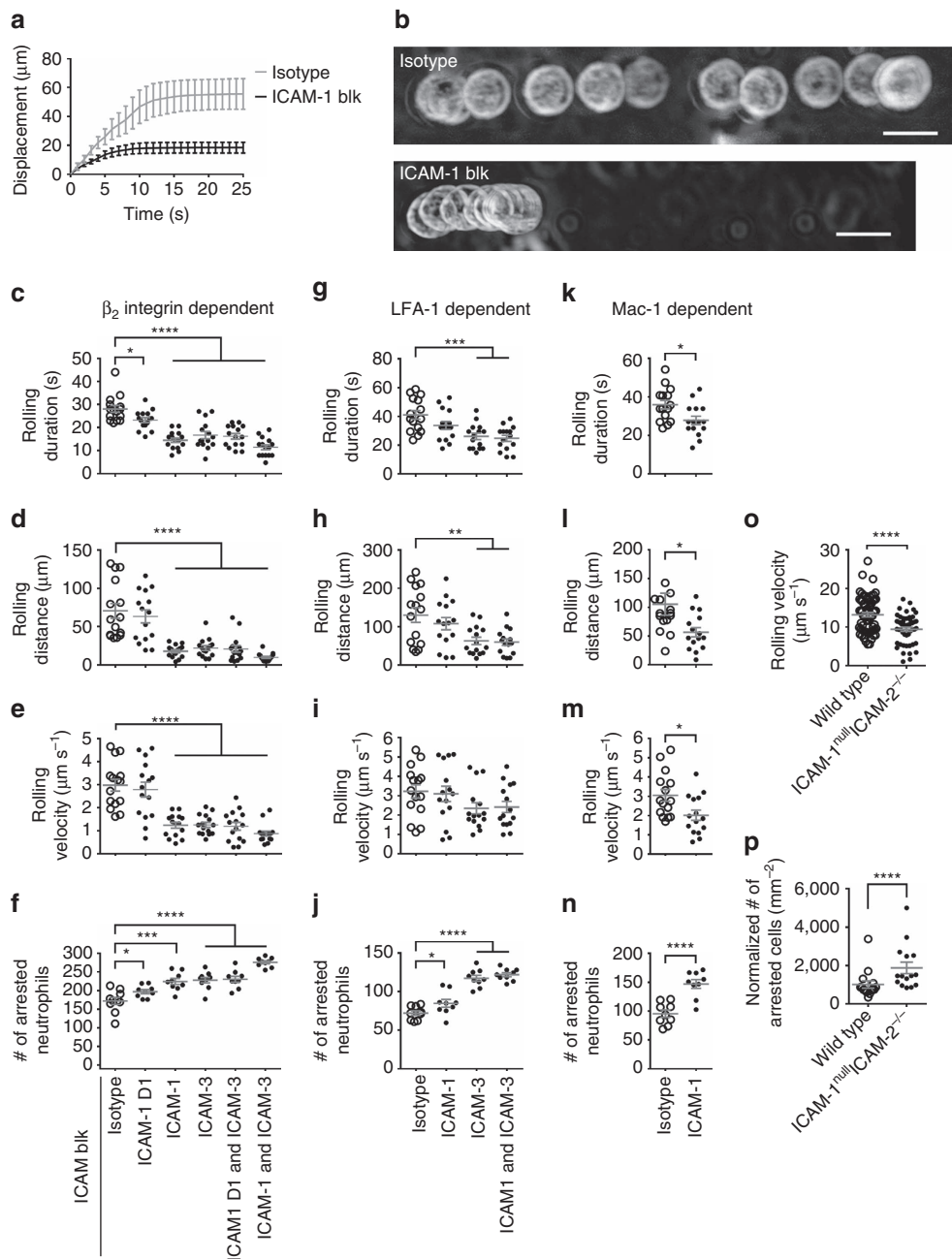


**Figure 7 | Blocking E<sup>-</sup>H<sup>+</sup> integrin binding to neutrophil ICAMs promotes leukocyte adhesion.** (a) Displacements of human neutrophils ( $n = 5$ ) with or without blockade of neutrophil ICAM-1 during rolling on P-selectin/ICAM-1/IL-8. (b) Maximum intensity projection of a typical bright-field-imaged human neutrophil with (13 frames) or without (30 frames) blockade of neutrophil ICAM-1 rolling on P-selectin/ICAM-1/IL-8. Flow direction is from left to right. Scale bar, 10  $\mu\text{m}$ . (c-f) Rolling duration until arrest (c,  $n = 15$  cells per group), rolling distance until arrest (d,  $n = 15$  cells per group), rolling velocity before arrest (e,  $n = 15$  cells per group) and the number of arrested human neutrophils (f,  $n = 9$  observations per group) with or without blockade of neutrophil ICAM-1 D1 (domain 1, binds LFA-1, mAb HA58), or ICAM-1 (binds both LFA-1 and Mac-1, mAbs HA58 and R6.5), and/or ICAM-3 (binds LFA-1, mAb CBR-IC3/1). (g-j) Upon blockade of Mac-1 by mAb ICRF44, LFA-1-dependent *cis* binding was analysed with or without blockade of LFA-1 *cis* binding to neutrophil ICAM-1 (mAb HA58), and/or ICAM-3 (mAb CBR-IC3/1).  $n = 15, 15, 15$  and 9 cells per group in g,h,i and j, respectively. (k-n) Upon blockade of LFA-1 (mAb TS1/22), Mac-1-dependent *cis* binding was analysed with or without blockade of Mac-1 *cis* binding to neutrophil ICAM-1 (mAb R6.5).  $n = 15, 15, 15$  cells, and nine observations per group in k,l,m and n. (o) Leukocyte rolling velocity ( $n = 48$  for ICAM-1<sup>null</sup>ICAM-2<sup>-/-</sup> and 65 for wild type<sup>DsRed</sup> cells) in mouse cremaster muscle venules of ICAM-1<sup>null</sup>ICAM-2<sup>-/-</sup>/wild type<sup>DsRed</sup> mixed chimeric mice before intravenous injection of CXCL1. (p) The number of adherent leukocytes ( $n = 15$  observations) in mouse cremaster muscle venules of the mixed chimeric mice 1 min after intravenous injection of 600 ng CXCL1. Mean values and s.e.m.s (error bars) were presented in a,c-p. \* $P < 0.05$ , \*\* $P < 0.01$ , \*\*\* $P < 0.001$ , \*\*\*\* $P < 0.0001$  in unpaired student t-test for a,c-o and paired student t-test for p.

freshly recruited Mac-1 can interact with ICAMs in *cis* is unknown.

An alternative possibility that would explain the observation of KIM127<sup>-</sup> mAb24<sup>+</sup> clusters is steric exclusion. If extended

integrin molecules were clustered so tightly that KIM127 cannot find its binding site, extended high-affinity integrin would be falsely classified as bent. If this were the case, clustered extended high-affinity integrin would be available to bind ligand in *trans*

and not available to bind ligand in *cis*. Therefore, the steric antibody exclusion hypothesis is not supported by our functional data (Figs 6 and 7 and Supplementary Fig. 12), which clearly show that liberating  $\beta_2$  integrins from interactions in *cis* increases binding to ligand in *trans* and consequently neutrophil adhesion and aggregation.

Our finding also suggests a possible new class of drugs that target  $\beta_2$  integrins. Currently, six integrin-targeting drugs are on the market, five of which are antibodies or small molecules that inhibit the ligand-binding site<sup>59</sup>. The present data suggest that a new class of allosteric inhibitors that stabilize  $E^-H^+$  may be useful as anti-inflammatory drugs. Conversely, molecules that release  $E^-H^+$  to  $E^+H^+$  could be used to fight infections where more neutrophil recruitment might be needed.

Beyond neutrophils,  $\beta_2$  integrins are widely expressed and functional in other leukocyte subsets. LFA-1 on lymphocytes is involved in trafficking to lymph nodes<sup>60</sup> and in the formation of the immunological synapse<sup>61</sup>. The newly discovered  $E^-H^+$  conformation thus may also be involved in the regulation of adaptive immunity. The recruitment of patrolling monocytes<sup>62</sup> is also  $\beta_2$  integrin-dependent. Finally, other integrins may also have  $E^-H^+$  conformations, which may be involved in other immunological processes, like  $\beta_1$  integrin-dependent<sup>60</sup> or  $\beta_7$  integrin-dependent<sup>63</sup> leukocyte recruitment.

In conclusion, we show that  $H^+E^- \beta_2$  integrins exist on rolling neutrophils, where they bind ICAM-1 in *cis*, thus limiting neutrophil adhesion by preventing ICAM-1 binding in *trans*. These data support a revised model of  $\beta_2$  integrin activation separating headpiece opening from extension (Supplementary Fig. 1). Beside the significance in  $\beta_2$  integrin activation during neutrophil adhesion in particular, our finding provides insights into integrin function in general.

## Methods

**Reagents.** Recombinant human P-selectin-Fc, ICAM-1-Fc and IL-8 were purchased from R&D Systems. Murine CXCL1 was purchased from Pepro Tech. Casein blocking buffer was purchased from Thermo Fisher Scientific. The conformation specific antibody mAb24 to human  $\beta_2$ -I-like-domain, which reports the headpiece-opening<sup>29–32</sup>, was purchased from Abcam. The KIM127 mAb to human  $\beta_2$ -IEGF-domain, which reports the ectodomain extension<sup>27,28</sup>, was purified at the Lymphocyte Culture Center at the University of Virginia from hybridoma supernatant (American Type Culture Collection). Purified CD11a blocking mAb TS1/22 was purchased from Thermo Fisher Scientific. Purified CD11b blocking mAb ICRF44, purified CD11a non-blocking mAb TS2/4, purified and FITC-conjugated ICAM-1 domain 1 mAb HA58, purified ICAM-3 blocking mAb CBR-IC3/1, purified ICAM-2 blocking mAb CBR-IC2/2, FITC-conjugated anti-mouse IgG1 mAb, and purified isotype control mAbs were purchased from Biolegend. The CD18 blocking mAb IB4, and human Fc receptor (FcR) blocking reagents were purchased from Miltenyi Biotec. Purified ICAM-1 domain 2 mAb R6.5 was purchased from eBioscience. FITC-conjugated CD14 mAb was purchased from Invitrogen. DL488- or DL550-conjugated isotype control mAbs were purchased from Novus Biologicals. FITC-conjugated isotype control mAbs was purchased from BD Bioscience. mAb24, KIM127 or TS2/4 were directly labelled by DL488 or DL550 using DyLight antibody labelling kits from Thermo Fisher Scientific. CellMask DeepRed was purchased from Molecular Probes. CellTrace CFSE and CellTracker Orange CMRA were purchased from Thermo Fisher Scientific. Quantum Simply Cellular anti-Mouse (calibration beads) was purchased from Bangs Laboratories. Polymorphprep was purchased from Accurate Chemical. Roswell Park Memorial Institute (RPMI) medium 1,640 without phenol red and phosphate-buffered saline (PBS) without  $Ca^{2+}$  and  $Mg^{2+}$  were purchased from Gibco. Human serum albumin (HSA) was purchased from Gemini Bio Products. Paraformaldehyde (PFA) was purchased from Thermo Fisher Scientific.

**Mice.** C57BL/6J wild-type mice (000664; JAX) and DsRed mice (006051; JAX; wild-type C57BL/6J background) were obtained from the Jackson Laboratory. Mice were fed a standard rodent chow diet and were housed in microisolator cages in a pathogen-free facility. Mice were euthanized by  $CO_2$  inhalation. All experiments followed guidelines of the La Jolla Institute for Allergy and Immunology Animal Care and Use Committee, and approval for use of rodents was obtained from the La Jolla Institute for Allergy and Immunology according to criteria outlined in the Guide for the Care and Use of Laboratory Animals from the National Institutes of Health.

ICAM-1<sup>null</sup> and ICAM-2<sup>-/-</sup> mice were described before<sup>31,52</sup>. They were backcrossed to the C57BL/6 background for at least eight generations<sup>64</sup>. ICAM-1

and ICAM-2 double-deficient (ICAM-1<sup>null</sup>/ICAM-2<sup>-/-</sup>) C57BL/6 mice were generated by crossing ICAM-1<sup>null</sup> and ICAM-2<sup>-/-</sup> C57BL/6 mice in the specific pathogen-free animal facility, University of Bern, Switzerland. Animal procedures were performed in accordance with the Swiss legislation on the protection of animals and approved by the veterinary office of the Kanton of Bern.

**Bone marrow transplantation for mixed chimera.** Recipient mice (C57BL/6J wild-type male, 8-weeks old, Jackson Labs) were irradiated in two doses of 550 rads each (for a total of 1,100 rads) 4 h apart. Bone marrow cells from both femurs and tibias of donor mice (ICAM-1<sup>null</sup>/ICAM-2<sup>-/-</sup> male and DsRed wild-type male, 11 weeks old) were collected under sterile conditions. Bones were centrifuged for the collection of marrow, unfractionated bone marrow cells were washed, resuspended in PBS, mixed at a ratio of 1:1 (2.5 million cells each) in 200  $\mu$ l, confirmed by flow cytometry and injected retro-orbitally into the lethally irradiated mice. Recipient mice were housed in a barrier facility under pathogen-free conditions before and after bone marrow transplantation. After bone marrow transplantation, mice were provided autoclaved acidified water with antibiotics (trimethoprim-sulfamethoxazole) and were fed autoclaved food. Mice were used for experiments 6 weeks after bone marrow reconstitution.

**Neutrophil isolation.** Heparinized whole blood was obtained from healthy human donors after informed consent, as approved by the Institutional Review Board of the La Jolla Institute of Allergy & Immunology in accordance with the Declaration of Helsinki. Informed consent was obtained from all donors. Neutrophils were isolated by using Polymorphprep (a mixture of sodium metrizoate and Dextran 500) density gradient. Briefly, human blood was applied onto Polymorphprep, centrifuged at 500g for 35 min at 20–25 °C, resulting in neutrophils concentrated in a layer between peripheral blood mononuclear cells and erythrocytes. After washing with PBS without  $Ca^{2+}$  and  $Mg^{2+}$  twice, the neutrophils (>95% purity by flow cytometry, no visible activation by microscopy) were re-suspended in RPMI-1640 without phenol red plus 2% HSA and were used within 4 h. Neutrophils were incubated with FcR blocking reagents for 10 min at room temperature before all the experiments.

**Microfluidic device.** The assembly of the microfluidic devices used in this study and the coating of coverslips with recombinant human P-selectin-Fc, ICAM-1-Fc and IL-8 has been described previously<sup>15,16,33</sup>. Briefly, coverslips were coated with P-selectin-Fc (2  $\mu$ g ml<sup>-1</sup>), ICAM-1-Fc (10  $\mu$ g ml<sup>-1</sup>), and IL-8 (10  $\mu$ g ml<sup>-1</sup>) for 2 h and then blocked for 1 h with casein (1%) at room temperature. In some experiments (Fig. 2), coverslips were coated with P-selectin-Fc only, P-selectin-Fc plus ICAM-1-Fc, or P-selectin-Fc plus IL-8. After coating, coverslips were sealed to polydimethylsiloxane chips by magnetic clamps to create flow chamber channels ~29  $\mu$ m high and ~300  $\mu$ m across. By modulating the pressure between the inlet well and the outlet reservoir, 6 dyn cm<sup>-2</sup> wall shear stress was applied in all experiments.

**Microfluidic perfusion assay.** To study the arrest of neutrophils, isolated human primary neutrophils ( $5 \times 10^6$  cells ml<sup>-1</sup>) were perfused in the microfluidic device over a substrate of recombinant human P-selectin-Fc with or without recombinant human ICAM-1-Fc and/or IL-8 under shear stress of 6 dyn cm<sup>-2</sup>. In some experiments (Supplementary Fig. 2a), neutrophils were incubated with anti-CD11a (TS1/22, blocking, 10  $\mu$ g ml<sup>-1</sup>) mAb, anti-CD11b (ICRF44, blocking, 10  $\mu$ g ml<sup>-1</sup>) mAb, anti-CD18 (IB4, blocking, 10  $\mu$ g ml<sup>-1</sup>) mAb for 20 min at room temperature before being perfused into the microfluidic devices, as described previously<sup>33</sup>. In some experiments (Supplementary Fig. 2b–e), neutrophils were incubated with isotype mAb (10  $\mu$ g ml<sup>-1</sup>), KIM127 and isotype (5  $\mu$ g ml<sup>-1</sup> each), mAb24 and isotype (5  $\mu$ g ml<sup>-1</sup> each) or KIM127 and mAb24 (5  $\mu$ g ml<sup>-1</sup> each) for 3 min at room temperature before being perfused into the microfluidic devices. In ICAM-1/ICAM-3 blocking experiments (Fig. 7c–n), neutrophils were incubated with ICAM-1 domain 1 blocking mAb HA58 (10  $\mu$ g ml<sup>-1</sup>), or/and domain 3 blocking mAb R6.5 (10  $\mu$ g ml<sup>-1</sup>), and/or ICAM-3 blocking mAb CBR-IC3/1 (10  $\mu$ g ml<sup>-1</sup>), or/and isotype control mAbs for 20 min at room temperature, with two washes before being perfused into the microfluidic devices. IB4, TS1/22 and ICRF44 mAbs were used in some data sets to assess the contribution of  $\beta_2$  integrins, LFA-1 and Mac-1 in the *cis* interactions. The microfluidic devices were perfused with neutrophils for 10 min and washed with RPMI-1640 without phenol red plus 2% HSA for 5 min. Then, the arrested neutrophils were counted in nine fields-of-view per group. In some experiments, time-lapse images (one frame per second) were taken during the perfusion. Then the rolling duration and rolling distance were acquired from the images by analysing 15 cells starting rolling to arrest.

**Homogeneous binding qDF imaging.** The homogeneous binding assay (that is, the continuous real-time measurement without separation of soluble antibody<sup>33</sup>) and qDF imaging<sup>15,16</sup> were combined here. Briefly, the conformation reporting antibody mAb24 or KIM127 were conjugated with DL488 or DL550, respectively, using the DyLight antibody labelling kits according to the manufacturer's instructions. In some experiments (Supplementary Fig. 7), the fluorochromes of mAb24 and KIM127 were switched to test for possible nonspecific effects of the

fluorochromes. In neutrophil ICAM-1 blocking experiments (Fig. 6), neutrophils were incubated with both ICAM-1 domain 1 mAb HA58 ( $10 \mu\text{g ml}^{-1}$ ) and domain 2 mAb R6.5 ( $10 \mu\text{g ml}^{-1}$ ), which will block both LFA-1 and Mac-1 binding<sup>49</sup>, or isotype control mAbs for 20 min at room temperature, with two washes before performing the homogeneous binding assay.

During the homogeneous binding assay, neutrophils ( $2.5 \times 10^6$  cells  $\text{ml}^{-1}$ ) were incubated with fluorochrome-conjugated reporting mAbs ( $5 \mu\text{g ml}^{-1}$  each) for 3 min at room temperature and immediately perfused through the microfluidic device at a wall shear stress of  $6 \text{ dyn cm}^{-2}$  without separation of the soluble mAbs. The plasma membrane of neutrophils was labelled with CellMask DeepRed according to the manufacturer's instructions before the incubation with mAbs. When neutrophils were observed rolling on the substrate, acquisition was started using TqDF microscopy to acquire the dynamics of integrin activation on neutrophil footprint during rolling ( $\sim 30$  s), arrest and  $\sim 30$ – $100$  s following arrest.

To assess the binding kinetics and stability of binding of the mAbs, neutrophils were perfused through the microfluidic device at a wall shear stress of  $6 \text{ dyn cm}^{-2}$  for 5 min to allow them to roll and arrest on the substrate. Then 1% PFA was perfused through the device to fix the neutrophils for 5 min. After washing the device by PBS perfusion for 5 min,  $5 \mu\text{g ml}^{-1}$  of fluorochrome-conjugated reporting mAbs KIM127 or mAb 24 were perfused through the device. Footprints of the fixed cells were recorded by TqDF microscopy.

**TqDF microscopy.** The qDF set up and the theory of qDF have been described previously in detail<sup>15</sup>. Here, we expended qDF to three channels (TqDF). The set up consisted of an IX71 inverted TIRF research microscope (Olympus America) with a  $100 \times$  NA 1.45 plan-apochromatic oil immersion TIRF microscopy objective and 10 mW blue ( $\lambda = 488 \text{ nm}$ ), 10 mW yellow-green ( $\lambda = 561 \text{ nm}$ ), and 5 mW red ( $\lambda = 641 \text{ nm}$ ) diode-pumped solid-state lasers (CVI Melles Griot) as TIRF excitation light sources. Images were captured at a rate of 0.2–1 frames per second using a QV2 (Photometrics) QuadView video coupler and a 16-bit digital charge coupled device camera (Hamamatsu C10600-10B ORCA-R2). The laser shutters and camera were controlled with the SlideBook5.5 software (Intelligent Imaging Innovations). The absorption and emission peaks of the fluorochromes used in this study were, respectively, 493 and 518 nm for DL488, 562 and 576 nm for DL550, 649 and 666 nm for CellMask DeepRed. There was no bleed-through between channels. A TIRF incidence angle of  $\theta = 70^\circ$  was used for all three lasers in all TqDF experiments.

**Intravital microscopy.** For *in vivo* imaging of leukocyte rolling and arrest, intravital microscopy of postcapillary venules of the cremaster muscle was performed on five mixed chimeric mice as described before<sup>36,41</sup>. Anesthesia was induced with an intraperitoneal injection of ketamine hydrochloride ( $125 \text{ mg kg}^{-1}$ ) and xylazine ( $12.5 \text{ mg kg}^{-1}$ ), and was maintained with inhalation of isoflurane/oxygen gas mixture. The left carotid artery was cannulated with a polyethylene-10 tube (BD) and the left cremaster muscle was exteriorized and prepared for imaging through a  $\times 20$  water immersion objective with simultaneous bright-field and epifluorescent imaging, where the wild-type (DsRed) leukocytes appeared bright and the ICAM-1<sup>null</sup>ICAM-2<sup>-/-</sup> leukocytes appeared dim. On each cremaster muscle, three different postcapillary venular sites with rolling leukocytes were recorded. After one minute of recording rolling, 600 ng murine CXCL1 was injected through the carotid cannula. The numbers of arrested DsRed wild-type and ICAM-1<sup>null</sup>ICAM-2<sup>-/-</sup> leukocytes were counted within 2 min after injections. The arrest counts were normalized by the number of rolling cells before murine-CXCL1 injection and the square of imaged venules.

**$\Delta$  map and footprint binary images.** The distance ( $\Delta$ ) from any region in the neutrophil footprint within  $\sim 200 \text{ nm}$  to the total internal reflective interface can be calculated from fluorescence intensity of membrane dye using the equation described previously<sup>15</sup>. Membrane fluorescence images (Supplementary Fig. 4a) were converted to  $\Delta$  maps (Supplementary Fig. 4b) that encode  $\Delta$  as pixel intensity, using the 'Math' function in FIJI-ImageJ2. The neutrophil footprint binary images were generated from  $\Delta$  maps by setting a threshold of 95 (the distance to the interface  $\leq 95 \text{ nm}$ , Supplementary Fig. 4c), which excluded the background not associated with the footprint. The footprint outline images (Fig. 1b,c,f, Supplementary Fig. 4d,g and Supplementary Movie 1) were generated from footprint binary images using the 'Outline' function in FIJI-ImageJ2.

**Displacements of the neutrophils and definition of the arrest.** The time-lapse footprint binary images were used to compute the cell velocities and displacements (Fig. 2a–d) using 'TrackMate' in FIJI-ImageJ2. Cell arrest was defined as the time when the velocity dropped below  $0.1 \mu\text{m s}^{-1}$ .

**Binary images of integrin clusters.** Binary images of integrin clusters (Fig. 1d–f, Fig. 3a, Fig. 4d–f, Fig. 6b, Supplementary Figs 4f,g and 7 and Supplementary Movies 1 and 2) were generated from raw images (Supplementary Figs 4e,5) by using 'Smart Segmentation' in ImagePro Premier 9.1 (Media Cybernetics), which is widely used for identifying objects<sup>55</sup>. Smart Segmentation is a pixel classification algorithm<sup>66</sup>, which uses reference objects to define classes based on pixel

intensities. Subsequently, each pixel in the image is analysed and compared with the values of the reference objects and the pixel is assigned to the class of the closest reference object. Different from simple thresholding, Smart Segmentation can identify clusters by comparing each cluster with its local background. Final binary images for integrin clusters (Supplementary Fig. 4g) were prepared by subtracting background noise not associated with neutrophil footprints using 'image calculator' in FIJI-ImageJ2.

Dual colour binary images of integrin clusters were split into binary images for yellow ( $E^+H^+$ ), red ( $E^+H^-$ ), and green ( $E^-H^+$ ) clusters, respectively. Raw images were masked with the binary clusters and mean fluorescence intensity was quantified using the 'analyze particles' function in FIJI-ImageJ2. The mean fluorescence intensities (MFI) were normalized by background intensities and highest fluorescence intensities in the recording. Quantification of the KIM127 and mAb24 MFI of yellow ( $E^+H^+$ , Supplementary Fig. 4h), red ( $E^+H^-$ , Supplementary Fig. 4i), or green ( $E^-H^+$ , Supplementary Fig. 4j) clusters demonstrated the accuracy of the cluster binary images generated by 'Smart Segmentation'. KIM127 and mAb24 MFI for each cluster were plotted against each other to identify the three populations of clusters (Supplementary Fig. 4k). To measure the cluster number (Fig. 2e–t, Fig. 4m, Fig. 6c–f, Supplementary Fig. 6a), total area (Supplementary Fig. 6b) and average size (Supplementary Fig. 6c), the cluster binary images were analysed by 'analyze particles' in FIJI-ImageJ2.

**Colour transition history of the clusters.** The cluster binary images were analysed manually to reveal the colour transition history (representing integrin conformation changes) of the clusters. We analysed the  $E^+H^+$  clusters after cell arrest. 15 clusters, which transitioned from  $E^+H^-$  clusters (Fig. 3b,c), and 15 clusters, which transitioned from  $E^-H^+$  clusters (Fig. 3d,e), were analysed by acquiring the pixel colours over 4 s. KIM127 and mAb24 fluorescence intensity of individual pixels in these clusters were analysed within these 4 s (Supplementary Fig. 8). In some analyses, 15 arrested cells were selected to reveal their colour transition history of the clusters (Fig. 3f). The colours when the clusters were first observed were defined as their initial colour. In some analyses, the durations of 16  $E^-H^+$  clusters each on ICAM-1 blocked or isotype mAb-treated neutrophils were calculated (Fig. 6g,h). The durations were the time from the appearing of the green clusters to appearing of yellow pixels in the clusters.

**Creation of 3D reconstructions/footprint topography.** Raw CellMask DeepRed qDF images were used to create 3D reconstructions (3D topography, Fig. 4a–f, Supplementary Fig. 9 and Supplementary Movie 2) by custom scripts in Matlab (MathWorks) as described previously<sup>15</sup>. Hills (microvilli) and valleys (the space between microvilli) were identified from CellMask DeepRed images by using 'Smart Segmentation' in ImagePro. Hills and valleys were pseudocoloured blue and magenta, respectively, to generate hill-valley maps (Fig. 4c, Supplementary Fig. 9) by custom scripts in Matlab.

**3D localization of the clusters.** To reveal the 3D localization of the clusters, the cluster binary images were superimposed on the 3D topography (Fig. 4d–f and Supplementary Movie 2) by custom scripts in Matlab. We masked the hill-valley maps and the  $\Delta$  maps with the yellow ( $E^+H^+$ ), red ( $E^+H^-$ ), or green ( $E^-H^+$ ) cluster areas, respectively, using 'image calculator' in FIJI-ImageJ2. The hill or valley location of each cluster was analysed by using 'measure' in FIJI-ImageJ2. Similarly, the  $\Delta$  of every cluster Fig. 4j–l) was analysed by the 'analyze particles' function in FIJI-ImageJ2.

**Integrin sites measurements.** To measure the integrin expression/epitope sites, we used QuantumTM Simply Cellular anti-Rat IgG beads coated with anti-rat IgG antibodies at five known antibody binding capacities. In all,  $10^6 \text{ ml}^{-1}$  human neutrophils were incubated with FcR blocking reagents for 10 min at room temperature, and then incubated with  $5 \mu\text{g ml}^{-1}$  KIM127, mAb24, which are both mouse anti-human IgG<sub>1</sub> isotype, and isotype control, respectively, for 5 min at room temperature. After fixation by 1% PFA on ice for 10 min, the cells were washed twice and incubated with FITC-conjugated rat anti-mouse IgG<sub>1</sub> mAb on ice for 30 min. The calibration beads were incubated with the same FITC-conjugated rat anti-mouse IgG<sub>1</sub> mAb according to the manufacturer's instruction. After measuring the fluorescence intensity of calibration beads, a linear correlation between the fluorescence intensity and antibody-binding sites was established.

KIM127 and mAb24 epitope sites on the footprint of rolling cells were determined by dividing the number of antibody molecules bound per cell by the cell surface and multiplying by the footprint area. Cell surface area was estimated based on the average diameter of 64 neutrophils captured by microscopy. The fluorescence intensity integral of both KIM127 and mAb24 on the footprint were calculated and converted to KIM127 and mAb24 epitope sites.

**FRET assay using flow cytometry.** Flow cytometry with compensation (BD FACSDiva) for bleed-through based FRET were used for detecting molecular interaction with high sensitivity<sup>55,67</sup>. To test whether  $E^-H^+$  integrin can interact with endogenous ICAM-1 in *cis*, FRET between  $H^+$  (mAb24-550 as acceptor) and ICAM-1 (domain 1 mAb HA58-FITC as donor) was measured. This assay tests the *cis* interaction of neutrophil ICAM-1 and  $E^-H^+$  Mac-1, which binds ICAM-1

domain 3. Isolated neutrophils ( $10^6$  cells  $\text{ml}^{-1}$ ) were incubated with FcR blocking reagents (1:100) for 10 min at room temperature, followed by incubating with  $5 \mu\text{g ml}^{-1}$  purified isotype control or mAb R6.5, which blocks Mac-1-ICAM-1 binding<sup>49</sup>, for 20 min at room temperature. Live cells were tested by time-resolved flow cytometry. The 488 nm laser excited the FRET donor HA58-FITC (525/50 nm), which excited the FRET acceptor mAb24-DL550 (575/25 nm).

To quantify the quenching of FRET donor fluorescence, HA58-FITC ( $2 \mu\text{g ml}^{-1}$ ) was added at 10 s after starting recording, with 3 min recording to reach saturation, followed by adding IL-8 ( $1 \mu\text{g ml}^{-1}$ ) inducing the mAb24 epitope (mAb24-DL550,  $5 \mu\text{g ml}^{-1}$ , Fig. 5b,d). mAb24-DL550 was replaced by vehicle, non-binding isotype control mAb (IgG<sub>1</sub>-DL550,  $5 \mu\text{g ml}^{-1}$ ) or KIM127-DL550 ( $5 \mu\text{g ml}^{-1}$ ), respectively, as negative controls. ICAM-1 blocked neutrophils served as control to test whether the blockade of Mac-1-ICAM-1 in *cis* interaction will eliminate the quenching of FRET donor HA58-FITC.

To quantify the increase in fluorescence of the FRET acceptor, IL-8 and mAb24-DL550 ( $1.5 \mu\text{g ml}^{-1}$ ) were added at 10 s after starting recording, with 3 min recording to reach saturation, followed by adding HA58-FITC ( $2 \mu\text{g ml}^{-1}$ , Fig. 5c,e). HA58-FITC was replaced by vehicle, isotype control mAb (IgG<sub>1</sub>-FITC,  $2 \mu\text{g ml}^{-1}$ ) or anti-CD14-FITC ( $2 \mu\text{g ml}^{-1}$ ), respectively, as negative controls. ICAM-1 blocked neutrophils served as control to test whether the blockade of Mac-1-ICAM-1 in *cis* interaction will eliminate the fluorescence increase of FRET acceptor mAb24-DL550.

**Distance calculation of the FRET pairs.** From the data obtained by the flow cytometry-based FRET assay, we obtain the value of FRET efficiency ( $E$ ) as

$$E = 1 - F'_D/F_D \quad (1)$$

in which  $F'_D$  and  $F_D$  is the fluorescence intensity of the FRET donor (FITC) in the presence and in the absence of the FRET acceptor (DL-550), respectively.

$E$  depends on the donor-to-acceptor separation distance  $r$  with an inverse sixth power law due to the dipole-dipole coupling mechanism:

$$E = \frac{1}{1 + (r/R_0)^6} \quad (2)$$

in which  $R_0$  is the Förster distance of this pair of donor and acceptor, defined as the distance at which the energy transfer efficiency is 50%.  $R_0$  depends on the overlap integral of the donor emission spectrum with the acceptor absorption spectrum and their mutual molecular orientation as expressed by the following equation:

$$R_0 = \frac{9(\ln 10)}{128\pi^5 N_A} \cdot \frac{Q_D \kappa^2}{\eta^4} \cdot J \quad (3)$$

in which  $N_A$  is Avogadro's number;  $Q_D$  is the fluorescence quantum yield of the donor in the absence of acceptor, which is 0.92 of FITC in physiological solutions<sup>68</sup>;  $\kappa^2$  is the dipole orientation factor (2/3 when both dyes are freely rotating and isotropically oriented);  $\eta$  (refractive index) of medium is  $\sim 1.338$  (ref. 69) and  $J$  is the spectral overlap integral of the donor-acceptor pair. The calculation of  $J$  was done by using a/e-ultraviolet-Vis-infrared Spectral Software 2.2 (FluorTools, www.fluortools.com). Spectra were obtained from Thermo Fisher Scientific.

**Aggregation assay using flow cytometry.** To assess whether the *cis* binding of  $\beta_2$  integrins to ICAMs affects neutrophil aggregation, we performed a flow cytometry based aggregation assay<sup>70</sup>. We separated isolated neutrophils into two populations labelled with CFSE and CMRA, respectively. Aggregation of a CFSE-labelled neutrophil with a CMRA-labelled neutrophil appears as a double-positive event in flow cytometry. ICAM-1 ( $10 \mu\text{g ml}^{-1}$  HA58 and  $10 \mu\text{g ml}^{-1}$  R6.5), ICAM-2 ( $10 \mu\text{g ml}^{-1}$  CBR-IC2/2) and ICAM-3 ( $10 \mu\text{g ml}^{-1}$  CBR-IC3/1) were all blocked (room temperature, 30 min) to eliminate the *cis* binding on CMRA population. In some experiments,  $\beta_2$  integrins on the CFSE population were blocked by  $10 \mu\text{g ml}^{-1}$  IB4 at room temperature for 30 min.

**Statistics.** Statistical analysis was performed with Prism 6 (GraphPad). Data (Fig. 2a–d,f–h,j–l,n–p,r–t, Fig. 3b–f, Fig. 4j–l, Fig. 5d,e, Fig. 6c–e,g, Fig. 7a,c–p, Supplementary Figs 2,3,4h–j and 6) are presented as mean  $\pm$  s.e.m. Single data points are presented in some graphs (Fig. 2e–t, Fig. 3f, Fig. 4j–m, Fig. 6c–h, Fig. 7c–p, Supplementary Fig. 2,4h–k and 6). The means for the data sets were compared using paired (Fig. 7p) or unpaired student *t*-tests with equal variances ( $n < 30$ , Fig. 2f–h,j–l,n–p, r–t, Fig. 3f, Fig. 4j–l, Fig. 5d,e, Fig. 6c–e,g, Fig. 7c–n, Supplementary Fig. 2) or Chi-square test ( $n \geq 30$ , Fig. 7o). Log-Gaussian, Gaussian and Lorentzian fits were applied, and the best fit for the data sets were shown in Fig. 6h. Linear regression fits were applied for the data sets in Fig. 2a–d, Fig. 4g–i, Fig. 6f. The slopes of the linear regression for the data sets in Fig. 4g–i were tested against zero and the slopes of the linear regression for the data sets in Fig. 6f were tested against each other using an *F*-test. *P* values  $< 0.05$  were considered significant. *Post hoc* analysis (SPSS 22.0 software, IBM) was performed to ensure that the sample size we chose had adequate power.

**Data availability.** The data that support the findings of this study are available from the corresponding author upon request.

## References

- Yipp, B. G. *et al.* Infection-induced NETosis is a dynamic process involving neutrophil multitasking *in vivo*. *Nat. Med.* **18**, 1386–1393 (2012).
- Taylor, P. R. *et al.* Activation of neutrophils by autocrine IL-17A-IL-17RC interactions during fungal infection is regulated by IL-6, IL-23, RORgammat and dectin-2. *Nat. Immunol.* **15**, 143–151 (2014).
- Iversen, M. B. *et al.* An innate antiviral pathway acting before interferons at epithelial surfaces. *Nat. Immunol.* **17**, 150–158 (2016).
- Chen, F. *et al.* Neutrophils prime a long-lived effector macrophage phenotype that mediates accelerated helminth expulsion. *Nat. Immunol.* **15**, 938–946 (2014).
- Autenrieth, S. E. *et al.* Depletion of dendritic cells enhances innate anti-bacterial host defense through modulation of phagocyte homeostasis. *PLoS Pathog.* **8**, e1002552 (2012).
- Barlic, J. *et al.* Regulation of tyrosine kinase activation and granule release through  $\beta$ -arrestin by CXCR1. *Nat. Immunol.* **1**, 227–233 (2000).
- Moser, M. *et al.* Kindlin-3 is required for  $\beta_2$  integrin-mediated leukocyte adhesion to endothelial cells. *Nat. Med.* **15**, 300–305 (2009).
- Zimmerli, W., Zarth, A., Gratwohl, A. & Speck, B. Neutrophil function and pyogenic infections in bone marrow transplant recipients. *Blood* **77**, 393–399 (1991).
- Lammermann, T. *et al.* Neutrophil swarms require LTB4 and integrins at sites of cell death *in vivo*. *Nature* **498**, 371–375 (2013).
- Camps, M. *et al.* Blockade of PI3K $\gamma$  suppresses joint inflammation and damage in mouse models of rheumatoid arthritis. *Nat. Med.* **11**, 936–943 (2005).
- Gunawan, M. *et al.* The methyltransferase Ezh2 controls cell adhesion and migration through direct methylation of the extranuclear regulatory protein talin. *Nat. Immunol.* **16**, 505–516 (2015).
- Pisitkun, P. *et al.* Interleukin-17 cytokines are critical in development of fatal lupus glomerulonephritis. *Immunity* **37**, 1104–1115 (2012).
- Ley, K., Laudanna, C., Cybulsky, M. I. & Nourshargh, S. Getting to the site of inflammation: the leukocyte adhesion cascade updated. *Nat. Rev. Immunol.* **7**, 678–689 (2007).
- Lawrence, M. B. & Springer, T. A. Leukocytes roll on a selectin at physiologic flow rates: distinction from and prerequisite for adhesion through integrins. *Cell* **65**, 859–873 (1991).
- Sundd, P. *et al.* Quantitative dynamic footprinting microscopy reveals mechanisms of neutrophil rolling. *Nat. Methods* **7**, 821–824 (2010).
- Sundd, P. *et al.* 'Slings' enable neutrophil rolling at high shear. *Nature* **488**, 399–403 (2012).
- Ostermann, G., Weber, K. S., Zerneck, A., Schroder, A. & Weber, C. JAM-1 is a ligand of the  $\beta_2$  integrin LFA-1 involved in transendothelial migration of leukocytes. *Nat. Immunol.* **3**, 151–158 (2002).
- Filippi, M. D. *et al.* Localization of Rac2 via the C terminus and aspartic acid 150 specifies superoxide generation, actin polarity and chemotaxis in neutrophils. *Nat. Immunol.* **5**, 744–751 (2004).
- Schnitzler, N., Haase, G., Podbielski, A., Lutticken, R. & Schweizer, K. G. A co-stimulatory signal through ICAM- $\beta_2$  integrin-binding potentiates neutrophil phagocytosis. *Nat. Med.* **5**, 231–235 (1999).
- von Andrian, U. H. *et al.* Two step model of leukocyte-endothelial cell interaction in inflammation: distinct roles for LECAM-1 and the leukocyte  $\beta_2$  integrins *in vivo*. *Proc. Natl Acad. Sci. USA* **88**, 7538–7542 (1991).
- DiVietro, J. A. *et al.* Immobilized IL-8 triggers progressive activation of neutrophils rolling *in vitro* on P-selectin and intercellular adhesion molecule-1. *J. Immunol.* **167**, 4017–4025 (2001).
- Smith, C. W., Marlin, S. D., Rothlein, R., Toman, C. & Anderson, D. C. Cooperative interactions of LFA-1 and Mac-1 with intercellular adhesion molecule-1 in facilitating adherence and transendothelial migration of human neutrophils *in vitro*. *J. Clin. Invest.* **83**, 2008–2017 (1989).
- Alon, R. & Feigelson, S. W. Chemokine-triggered leukocyte arrest: force-regulated bi-directional integrin activation in quantal adhesive contacts. *Curr. Opin. Cell Biol.* **24**, 670–676 (2012).
- Laudanna, C. & Alon, R. Right on the spot. Chemokine triggering of integrin-mediated arrest of rolling leukocytes. *Thromb. Haemost.* **95**, 5–11 (2006).
- Luo, B. H., Carman, C. V. & Springer, T. A. Structural basis of integrin regulation and signaling. *Annu. Rev. Immunol.* **25**, 619–647 (2007).
- Fan, Z. & Ley, K. Leukocyte arrest: biomechanics and molecular mechanisms of  $\beta_2$  integrin activation. *Biorheology* **52**, 353–377 (2015).
- Robinson, M. K. *et al.* Antibody against the Leu-CAM b-chain (CD18) promotes both LFA-1-dependent and CR3-dependent adhesion events. *J. Immunol.* **148**, 1080–1085 (1992).
- Lu, C., Ferzly, M., Takagi, J. & Springer, T. A. Epitope mapping of antibodies to the C-terminal region of the integrin  $\beta_2$  subunit reveals regions that become exposed upon receptor activation. *J. Immunol.* **166**, 5629–5637 (2001).
- Kamata, T. *et al.* The role of the CPNKEK sequence in the  $\beta_2$  subunit I domain in regulation of integrin  $\alpha_1\beta_2$  (LFA-1). *J. Immunol.* **168**, 2296–2301 (2002).
- Lu, C., Shimaoka, M., Zang, Q., Takagi, J. & Springer, T. A. Locking in alternate conformations of the integrin  $\alpha_1\beta_2$  I domain with disulfide bonds reveals

- functional relationships among integrin domains. *Proc. Natl Acad. Sci. USA* **98**, 2393–2398 (2001).
31. Yang, W., Shimaoka, M., Chen, J. & Springer, T. A. Activation of integrin  $\beta$ -subunit I-like domains by one-turn C-terminal  $\alpha$ -helix deletions. *Proc. Natl Acad. Sci. USA* **101**, 2333–2338 (2004).
  32. Dransfield, I. & Hogg, N. Regulated expression of  $Mg^{2+}$  binding epitope on leukocyte integrin  $\alpha$  subunits. *EMBO J.* **8**, 3759–3765 (1989).
  33. Kuwano, Y., Spelten, O., Zhang, H., Ley, K. & Zarbock, A. Rolling on E- or P-selectin induces the extended but not high-affinity conformation of LFA-1 in neutrophils. *Blood* **116**, 617–624 (2010).
  34. Zarbock, A., Lowell, C. A. & Ley, K. Spleen tyrosine kinase Syk is necessary for E-selectin-induced  $\alpha_1\beta_2$  integrin mediated rolling on intercellular adhesion molecule-1. *Immunity* **26**, 773–783 (2007).
  35. Stadtmann, A. *et al.* The PSGL-1-L-selectin signaling complex regulates neutrophil adhesion under flow. *J. Exp. Med.* **210**, 2171–2180 (2013).
  36. Zarbock, A., Deem, T. L., Burcin, T. L. & Ley, K.  $G\alpha_{12}$  is required for chemokine-induced neutrophil arrest. *Blood* **110**, 3773–3779 (2007).
  37. Montresor, A. *et al.* JAK tyrosine kinases promote hierarchical activation of Rho and Rap modules of integrin activation. *J. Cell Biol.* **203**, 1003–1019 (2013).
  38. Lagarrigue, F. *et al.* A RIAM/lamellipodin-talin-integrin complex forms the tip of sticky fingers that guide cell migration. *Nat. Commun.* **6**, 8492 (2015).
  39. Yang, J. *et al.* Conformational activation of talin by RIAM triggers integrin-mediated cell adhesion. *Nat. Commun.* **5**, 5880 (2014).
  40. Tadokoro, S. *et al.* Talin binding to integrin beta tails: a final common step in integrin activation. *Science* **302**, 103–106 (2003).
  41. Lefort, C. T. *et al.* Distinct roles for talin-1 and kindlin-3 in LFA-1 extension and affinity regulation. *Blood* **119**, 4275–4282 (2012).
  42. Campbell, I. D. & Humphries, M. J. Integrin structure, activation, and interactions. *Cold Spring Harb. Perspect. Biol.* **3**, a004994 (2011).
  43. Dustin, M. L. & Shaw, A. S. Costimulation: building an immunological synapse. *Science* **283**, 649–650 (1999).
  44. Bruehl, R. E., Springer, T. A. & Bainton, D. F. Quantitation of L-selectin distribution on human leukocyte microvilli by immunogold labeling and electron microscopy. *J. Histochem. Cytochem.* **44**, 835–844 (1996).
  45. Borregaard, N. *et al.* Changes in subcellular localization and surface expression of L-selectin, alkaline phosphatase, and Mac-1 in human neutrophils during stimulation with inflammatory mediators. *J. Leukoc. Biol.* **56**, 80–87 (1994).
  46. Staunton, D. E., Dustin, M. L., Erickson, H. P. & Springer, T. A. The arrangement of the immunoglobulin-like domains of ICAM-1 and the binding sites for LFA-1 and rhinovirus. *Cell* **61**, 243–254 (1990).
  47. Diamond, M. S., Garcia-Aguilar, J., Bickford, J. K., Corbi, A. L. & Springer, T. A. The I domain is a major recognition site on the leukocyte integrin Mac-1 (CD11b/CD18) for four distinct adhesion ligands. *J. Cell Biol.* **120**, 1031–1043 (1993).
  48. Barnard, A. L., Igakura, T., Tanaka, Y., Taylor, G. P. & Bangham, C. R. Engagement of specific T-cell surface molecules regulates cytoskeletal polarization in HTLV-1-infected lymphocytes. *Blood* **106**, 988–995 (2005).
  49. Diamond, M. S. *et al.* ICAM-1 (CD54): a counter-receptor for Mac-1 (CD11b/CD18). *J. Cell Biol.* **111**, 3129–3139 (1990).
  50. Woodfin, A. *et al.* ICAM-1-expressing neutrophils exhibit enhanced effector functions in murine models of endotoxemia. *Blood* **127**, 898–907 (2016).
  51. Bullard, D. C. *et al.* Intercellular adhesion molecule-1 expression is required on multiple cell types for the development of experimental autoimmune encephalomyelitis. *J. Immunol.* **178**, 851–857 (2007).
  52. Gerwin, N. *et al.* Prolonged eosinophil accumulation in allergic lung interstitium of ICAM-2 deficient mice results in extended hyperresponsiveness. *Immunity* **10**, 9–19 (1999).
  53. Adair, B. D. *et al.* Three-dimensional EM structure of the ectodomain of integrin  $\alpha_v\beta_3$  in a complex with fibronectin. *J. Cell Biol.* **168**, 1109–1118 (2005).
  54. Sen, M., Yuki, K. & Springer, T. A. An internal ligand-bound, metastable state of a leukocyte integrin,  $\alpha_x\beta_2$ . *J. Cell Biol.* **203**, 629–642 (2013).
  55. Gupta, V. *et al.* The  $\beta$ -tail domain ( $\beta$ TD) regulates physiologic ligand binding to integrin CD11b/CD18. *Blood* **109**, 3513–3520 (2007).
  56. Zarbock, A., Singbartl, K. & Ley, K. Complete reversal of acid-induced acute lung injury by blocking of platelet-neutrophil aggregation. *J. Clin. Invest.* **116**, 3211–3219 (2006).
  57. Kirschenbaum, L. A., Aziz, M., Astiz, M. E., Saha, D. C. & Rackow, E. C. Influence of rheologic changes and platelet-neutrophil interactions on cell filtration in sepsis. *Am. J. Respir. Crit. Care Med.* **161**, 1602–1607 (2000).
  58. Nijm, J., Wikby, A., Tompa, A., Olsson, A. G. & Jonasson, L. Circulating levels of proinflammatory cytokines and neutrophil-platelet aggregates in patients with coronary artery disease. *Am. J. Cardiol.* **95**, 452–456 (2005).
  59. Ley, K., Rivera-Nieves, J., Sandborn, W. J. & Shattil, S. Integrin-based therapeutics: biological basis, clinical use and new drugs. *Nat. Rev. Drug Discov.* **15**, 173–183 (2016).
  60. Ledgerwood, L. G. *et al.* The sphingosine 1-phosphate receptor 1 causes tissue retention by inhibiting the entry of peripheral tissue T lymphocytes into afferent lymphatics. *Nat. Immunol.* **9**, 42–53 (2008).
  61. Katagiri, K., Maeda, A., Shimonaka, M. & Kinashi, T. RAP1, a Rap1-binding molecule that mediates Rap1-induced adhesion through spatial regulation of LFA-1. *Nat. Immunol.* **4**, 741–748 (2003).
  62. Auffray, C. *et al.* Monitoring of blood vessels and tissues by a population of monocytes with patrolling behavior. *Science* **317**, 666–670 (2007).
  63. Peer, D., Park, E. J., Morishita, Y., Carman, C. V. & Shimaoka, M. Systemic leukocyte-directed siRNA delivery revealing cyclin D1 as an anti-inflammatory target. *Science* **319**, 627–630 (2008).
  64. Gorina, R., Lyck, R., Vestweber, D. & Engelhardt, B.  $\beta_2$  integrin-mediated crawling on endothelial ICAM-1 and ICAM-2 is a prerequisite for transcellular neutrophil diapedesis across the inflamed blood-brain barrier. *J. Immunol.* **192**, 324–337 (2014).
  65. Shaw, T. N. *et al.* Perivascular arrest of CD8+ T Cells is a signature of experimental cerebral malaria. *PLoS Pathog.* **11**, e1005210 (2015).
  66. Cheng, H. D., Jiang, X. H., Sun, Y. & Wang, J. Color image segmentation: advances and prospects. *Pattern Recogn.* **34**, 2259–2281 (2001).
  67. Chigae, A. *et al.* FRET detection of lymphocyte function-associated antigen-1 conformational extension. *Mol. Biol. Cell* **26**, 43–54 (2015).
  68. Fleming, G. R., Knight, A. W. E., Morris, J. M., Morrison, R. J. S. & Robinson, G. W. Picosecond fluorescence studies of xanthene dyes. *J. Am. Chem. Soc.* **99**, 4306–4311 (1977).
  69. Chan, C. J., Whyte, G., Boyde, L., Salbreux, G. & Guck, J. Impact of heating on passive and active biomechanics of suspended cells. *Interface Focus* **4**, 20130069 (2014).
  70. Neelamegham, S., Taylor, A. D., Shankaran, H., Smith, C. W. & Simon, S. I. Shear and time-dependent changes in Mac-1, LFA-1, and ICAM-3 binding regulate neutrophil homotypic adhesion. *J. Immunol.* **164**, 3798–3805 (2000).

## Acknowledgements

This research was supported by funding from the National Institutes of Health, USA (NIH, HL078784) and WSA postdoctoral fellowship from the American Heart Association, USA (AHA, 16POST31160014). We acknowledge Dr Michael Abadier from the Division of Inflammation Biology, La Jolla Institute for Allergy and Immunology for finding the ICAM-1/2 double knockout mice. We acknowledge Jackie Miller from the Division of Inflammation Biology, La Jolla Institute for Allergy and Immunology for preparing materials for bone marrow transplantation and mouse husbandry. We thank Dr Terry Sasser from Thermo Fisher Scientific for providing the excitation spectrum of DL550.

## Author contributions

Experiments were designed by Z.F. and K.L. Most of the experiments were performed by Z.F. *In vivo* cremaster imaging was performed by A.M. Data analysis was performed by Z.F. Image processing was performed by Z.F., S.M. and Z.M. FRET distance calculation was performed by Z.F. and S.M. Some of the custom scripts on MatLab were coded by S.M. The microfluidic device was designed by E.G. and A.G. The bones of ICAM-1/2 double-deficient mice were provided by B.E. and U.D. The manuscript was written by Z.F., K.L. and M.G. The project was supervised by K.L. All authors discussed the results and commented on the manuscript.

## Additional information

**Supplementary Information** accompanies this paper at <http://www.nature.com/naturecommunications>

**Competing financial interests:** The authors declare no competing financial interests.

**Reprints and permission** information is available online at <http://npg.nature.com/reprintsandpermissions/>

**How to cite this article:** Fan, Z. *et al.* Neutrophil recruitment limited by high-affinity bent  $\beta_2$  integrin-binding ligand in *cis*. *Nat. Commun.* **7**:12658 doi: 10.1038/ncomms12658 (2016).



This work is licensed under a Creative Commons Attribution 4.0 International License. The images or other third party material in this article are included in the article's Creative Commons license, unless indicated otherwise in the credit line; if the material is not included under the Creative Commons license, users will need to obtain permission from the license holder to reproduce the material. To view a copy of this license, visit <http://creativecommons.org/licenses/by/4.0/>

© The Author(s) 2016